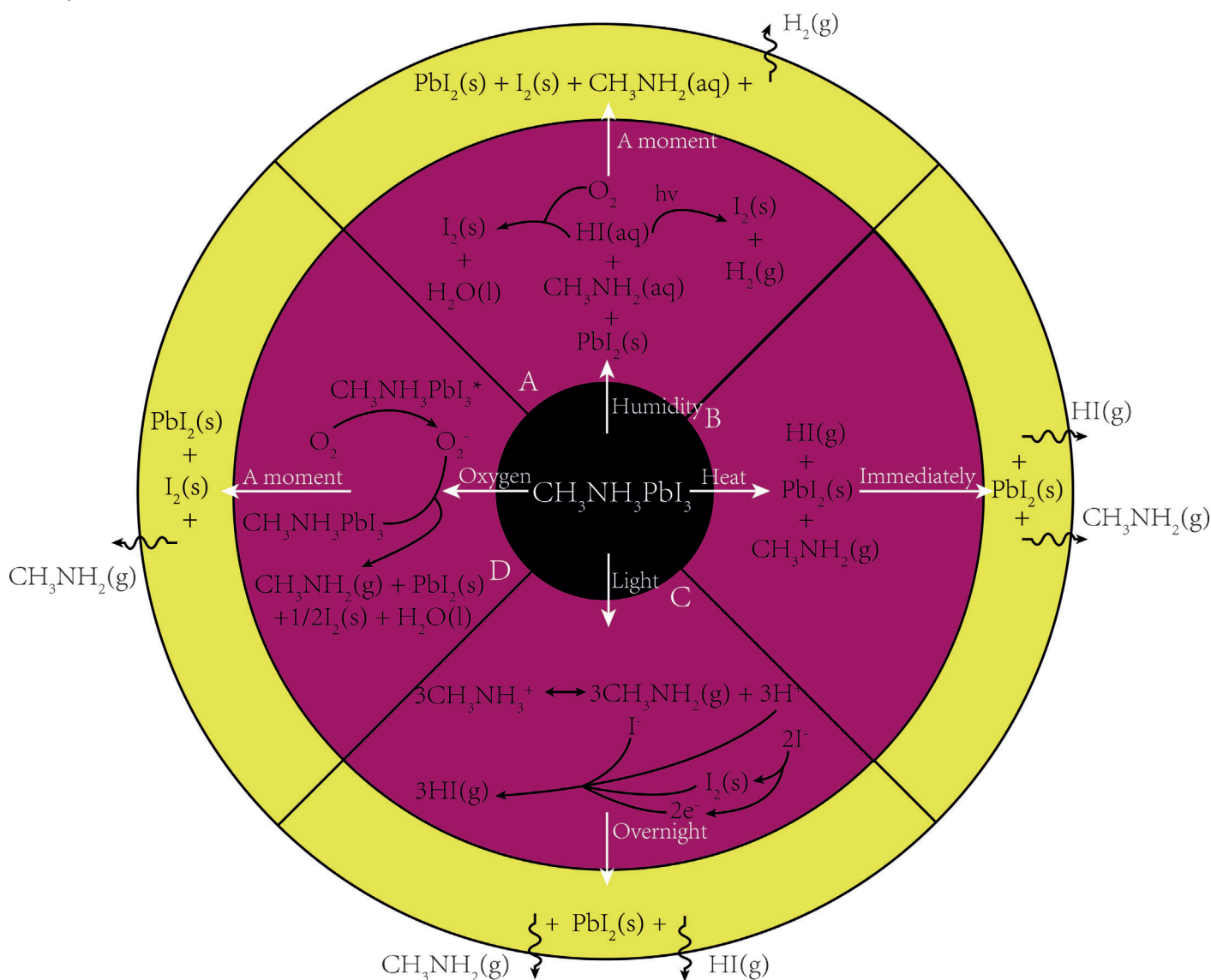


Stability of Perovskite Solar Cells: A Prospective on the Substitution of the A Cation and X Anion

Ze Wang, Zejiao Shi, Taotao Li, Yonghua Chen,* and Wei Huang*

Keywords:

organic/inorganic hybrid composites ·
perovskites · solar cells ·
stability · substitution



In recent years, organometal trihalide perovskites have emerged as promising materials for low-cost, flexible, and highly efficient solar cells. Despite their processing advantages, before the technology can be commercialized the poor stability of the organic–inorganic hybrid perovskite materials with regard to humidity, heat, light, and oxygen has to be overcome. Herein, we distill the current state-of-the-art and highlight recent advances in improving the chemical stability of perovskite materials by substitution of the A-cation and X-anion. Our hope is to pave the way for the rational design of perovskite materials to realize perovskite solar cells with unprecedented improvement in stability.

1. Introduction

With the rapid growth of the world's energy demand, the traditional fossil energy is increasingly unable to meet our energy needs and especially not in terms of clean, adequate, efficient, and safe energy solutions. Solar energy, inexhaustible and clean without any pollution has become one of the most potential avenues of new energy. The solar cell is a photoelectric device which can directly convert solar energy into electric energy, and offers the advantages of high light absorbing capacity, long cycle life, and low maintenance requirements. Since the first silicon single-crystal p–n junction solar cell was published by Bell Telephone Laboratories in 1954,^[1] the study of solar cells has exponentially increased over half a century moving from crystalline silicon solar cells to inorganic thin-film solar cells and dye-sensitized/polymer solar cells.^[2] Recently, a new generation of thin-film photovoltaic cells based on hybrid organic–inorganic metal halide perovskite absorbers has emerged. This new generation exhibits high efficiencies, exceeding 20 % in 2015^[3] and 22 % in 2016,^[4] surpassing by a large margin the organic photovoltaics and rivaling established photovoltaic technologies based on Si, CdTe, CuInGaSe, and GaAs.

Perovskites are solids with an ABX_3 composition in which X is an anion and A and B are cations of different sizes (A being larger than B, e.g., $A = CH_3NH_3^+$, $CH(NH_2)_2^+$, Cs^+ ; $B = Pb^{2+}$, Sn^{2+} ; $X = Cl^-$, Br^- , I^-).^[5] The B and X ions form MX_6^{4-} octahedra. The A cation is located in the cavity between the four MX_6^{4-} octahedra and is surrounded by 12 nearest neighbors. Their crystallographic stability and probable structure is preliminarily deduced by a tolerance factor t and an octahedral factor μ .^[6] The t can be expressed as $t = (r_A + r_X)/[\sqrt{2}(r_B + r_X)]$ and μ is defined as the ratio of r_B/r_X , where r_A , r_B , and r_X are the radius of cations A, metals ions B, and anions X, respectively.^[7] For halide perovskites ($X = F$, Cl , Br , I), $0.81 < t < 1.11$ and $0.44 < \mu < 0.90$ are generally required for a stable perovskite structure. If t lies in the narrower range 0.89–1.0, the cubic structure is more possible, while lower t values give less-symmetric tetragonal or orthorhombic structures. The μ value usually determines the stability of the octahedral phase and thus the stability of the perovskite structure. Currently, the t and μ values of the most widely used perovskite $CH_3NH_3PbI_3$ are 0.834 and 0.541,

respectively ($r_A = 180$ pm, $r_B = 119$ pm, $r_X = 220$ pm). By entirely or partly introducing ions with different sizes, the t and μ values can be adjusted and thus a more stable crystal structure could be obtained. The ionic radius is not the only factor that has an effect on the perovskite crystal phase, temperature has a great influence on whether a perovskite will form. Taking $CH_3NH_3PbI_3$ as an example, the orthogonal phase dominates at low temperature while the tetragonal and cubic phases dominate at temperatures higher than 162 K and 330 K, respectively.^[8,9]

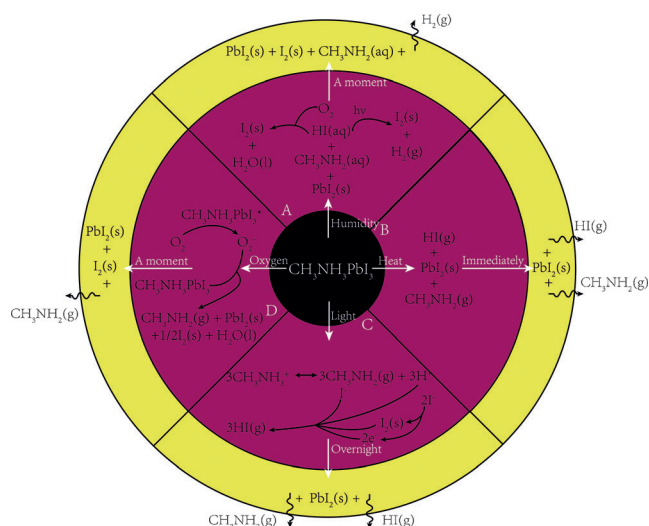
The development of perovskite solar cells has focused on two important issues with respect to practical applications. One is photoelectric conversion efficiency (PCE) and the other is stability.^[10,11] The PCE has been increased from less than 4 % to over 22.1 % in just a few years^[4,12] through device engineering and materials design based on the desired optoelectronic properties, for example, broad spectral absorption,^[5] high charge carrier mobility,^[13] small exciton binding energy (ca. 50 meV),^[14] and long exciton diffusion length.^[15,16] The PCEs of perovskite solar cells are now competitive with those of traditional crystalline solar cells, thus concern has recently turned to the long-term operational stability of perovskite solar cells with exposure to prolonged humidity, heat, light, and oxygen. To be marketable within the industry, perovskite solar cells must be able to operate continuously for close to 25 years in outdoor conditions.^[17] More research has been done on the long-term stability, with increased recognition of instability of the component materials under humidity, heat, light, and oxygen,^[18–25] as shown in Scheme 1. Perovskite materials most often suffer from a rapid degradation upon exposure to humidity.^[9,26–28] This process also appears to be accelerated by heat. The possible mechanisms of decomposition in moisture may be as follows [Eq. (1)–(4)].^[29]

[*] Z. Wang, Z. Shi, T. Li, Prof. Y. Chen, Prof. W. Huang
Key Laboratory of Flexible Electronics (KLOFE) & Institute of Advanced Materials (IAM), Jiangsu National Synergistic Innovation Center for Advanced Materials (SICAM)
Nanjing Tech University (NanjingTech)
30 South Puzhu Road, Nanjing 211816 (P.R. China)
E-mail: iamychen@njtech.edu.cn
wei-huang@njtech.edu.cn

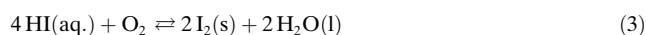
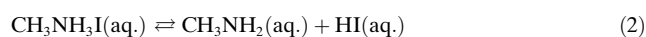
From the Contents

1. Introduction	3
2. Effect of the A Cation and Its Substitution on Stability	5
3. The Effect of Substitution of the X Anion on Stability	16
4. Conclusions and Outlook	21



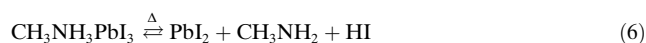
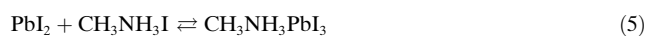


Scheme 1. The decomposition route of perovskite materials under A) humidity, B) heat, C) light, and D) oxygen.

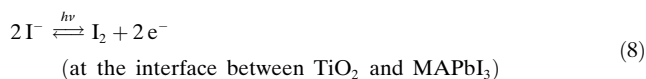
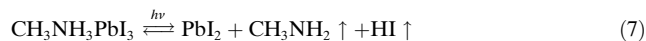


Interestingly, Walsh et al. demonstrated a novel idea that trace amounts of water in a closed system caused the hybrid perovskite to partially decompose.^[30] In their theory, H_2O is regarded as a Lewis base. Once the perovskite is exposed to water, the proton of ammonium in $\text{CH}_3\text{NH}_3\text{PbI}_3$ will coordinate with H_2O to an intermediate $[(\text{CH}_3\text{NH}_3^+)_{n-1}(\text{CH}_3\text{NH}_2)_n\text{PbI}_3][\text{H}_3\text{O}]$. Then the intermediate will continue to decompose into HI, CH_3NH_2 , and solid PbI_2 .

In addition, at temperatures higher than 150°C , the perovskite readily decomposes due in an endothermic reaction into its components PbI_2 , CH_3NH_2 , and HI.^[9,31–34] The decomposition reaction of the perovskite is the reverse reaction of perovskite formation, [Eq. (5),(6)]:

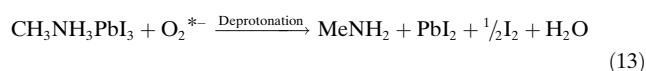


While the instability caused by humidity and heat are commonly observed in a wide range of hybrid perovskites, the current class of hybrid perovskites faces another challenge: they are unstable to light illumination.^[35–39] The possible mechanism of decomposition on exposure to light is as follows [Eq. (7)–(10)]:



On exposure to light, TiO_2 as an electron transport layer, can extract electrons from I^- , oxidizing I^- to iodine and the perovskite crystal structure is deconstructed. At the same time, methylammonium ion loses a proton, resulting in methylamine gas. Finally, iodine acquires electrons and combines with protons to generate HI gas.

Moreover, when exposed to both light and dry air the $\text{CH}_3\text{NH}_3\text{PbI}_3$ photoactive layers could rapidly decompose into a Al_2O_3 mesoporous structure yielding CH_3NH_2 , PbI_2 , and I_2 as products.^[40,41] Since the methylammonium component in $\text{CH}_3\text{NH}_3\text{PbI}_3$ has acidic protons, the degradation is initiated by the reaction of superoxide (O_2^-) with the methylammonium moiety of the perovskite absorber. The possible mechanism of decomposition by light is as follows [Eq. (11)–(13)]:



The degradation of the $\text{Al}_2\text{O}_3/\text{CH}_3\text{NH}_3\text{PbI}_3$ sample in a moisture-free environment can be accounted for by the generation of superoxide through electron transfer from the photoexcited perovskite phase to molecular oxygen. The



Wei Huang received his Ph.D. in Chemistry from Peking University in 1992. In 1993, he did postdoctoral research in the Chemistry Department at the National University of Singapore, and participated in the founding of the Institute of Materials Research and Engineering (A*STAR). In 2001, he became a chair professor at Fudan University, where he founded the Institute of Advanced Materials. In 2006, he became Deputy President of Nanjing University of Posts and Telecommunications, where he founded the Institute of Advanced Materials and the Key Laboratory for Organic Electronics and Information Displays. In 2012, he became President of Nanjing University of Technology.



Yonghua Chen received his Ph.D. in polymer chemistry and physics at the Changchun Institute of Applied Chemistry, Chinese Academy of Sciences, in 2011. After two-year postdoctoral research at Wake Forest University and two-year postdoctoral research at Case Western Reserve University, he is currently a full professor in Nanjing Tech University. His research interests are organic and organic/inorganic hybrid optoelectronic materials and devices for flat panel displays and solid-state lighting, and polymer and perovskite solar cells for energy conversion.

deprotonation of the methylammonium cation ultimately leads to the formation of CH_3NH_2 , PbI_2 , I_2 , and H_2O . Further, the resulting water could then participate in further degradation pathways as shown above.

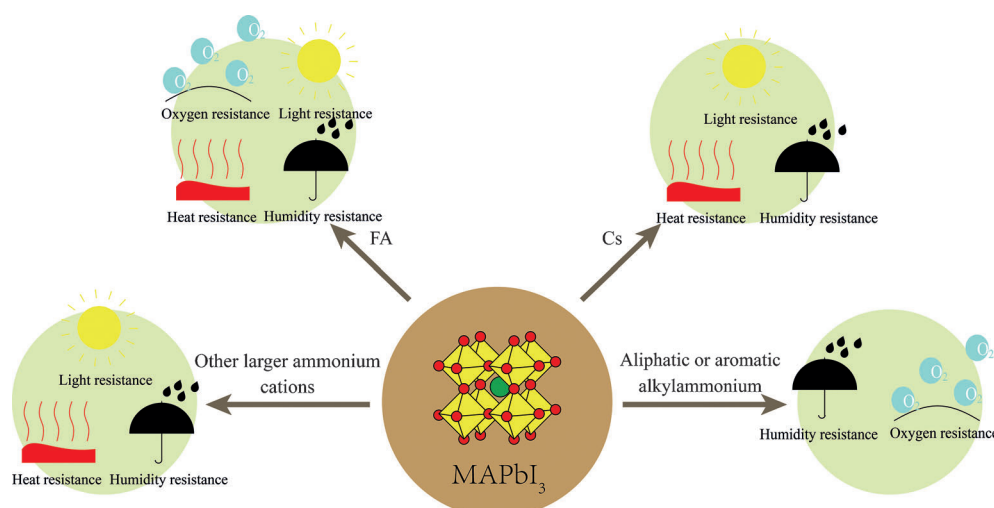
The above discussion leaves no question that moisture is a critical cause of instability of perovskite materials in devices. This extreme vulnerability to moisture has spurred efforts to make the top charge-transporting layer of the device the first line of defense against moisture ingress. We can differentiate between several approaches: the employment of a thin blocking layer between the perovskite and the hole- or electron-transporting material,^[27,42–48] the use of hydrophobic polymer or metal oxide hole- and electron-transporting layers,^[49–72] the use of hydrophobic carbon electrodes,^[73–79] and some others special methods.^[80–88] The approaches significantly improve the stability of perovskite solar cells by device engineering. However, these require careful design of charge-transporting materials and the light- and heat-induced instability issues remain. Recently, more research focuses on the modification of perovskite materials to improve the stability of perovskites themselves since a small lattice expansion or distortion will cause a symmetry change that will give structural stability to the material. In addition, the device performance can also be simultaneously improved.

Herein, we focus on recent advances to improve the chemical stability of perovskite materials through substitution of the A-cation and X-anion. The aim is to open new perspectives for the rational design of perovskite materials to create perovskite solar cells with unprecedented stability. We hope this approach will help the reader understand the issues of substitution of the A-cation and X-anion which affect the stability of perovskite solar

cells. We believe our insights will provide useful information to the community for the development of reasonably stable and high-PCE perovskite solar cells for outdoor applications in the near future.

2. Effect of the A Cation and Its Substitution on Stability

The A cation (e.g., $\text{CH}_3\text{NH}_3^+(\text{MA}^+)$, $\text{CH}(\text{NH}_2)_2^+(\text{FA}^+)$, Cs^+) occupies the central position of the 3D perovskite structure which is a key part of the perovskite that determines its structure and dimensionality. It has a direct influence on the stability and opto-electronic properties of the material. To effectively substitute the A cation and keep or improve the device performance, we will to work within the constraint that the cavity between four vertex sharing BX_6 octahedra only permits, with respect to a tolerance factor, the incorporation of cations with similar radii to the original cation into the 3D perovskite structure. The aim of substituting the A cation is to obtain a more-stable cubic phase and the appropriate dynamic position of the conduction band of the perovskite films, which plays a major role in improving the stability.^[89]



Scheme 2. Effect of cations and their substitutions on the stability of perovskite materials.



Ze Wang received the B.E. degree in applied chemistry from University of Science and Technology of Anhui in 2015. He is currently a Ph.D. student in the Institute of Advanced Materials (IAM), Nanjing Tech University under the supervision of Professor Yonghua Chen. His research is focused on the stability of metal halide perovskite solar cells.

However, to date only a restricted range of cations were investigated and shown to give stable and evenly distorted 3D perovskite structure (Scheme 2).

2.1. Effect of the FA Cation

The most investigated organic cation counterpart for the substitution of the MA^+ ion has been the FA^+ ion, which gives rise to a t value of 0.88, higher than the t value of 0.83 for MAPbI_3 .^[90] Baikie and Mathews et al. reported FAPbI_3 perovskite for the first time.^[91] FAPbI_3 perovskite has a similar crystal structure to MAPbI_3 (Figure 1A). Moreover, compared to MA^+ , FA^+ has a relatively large radius and was



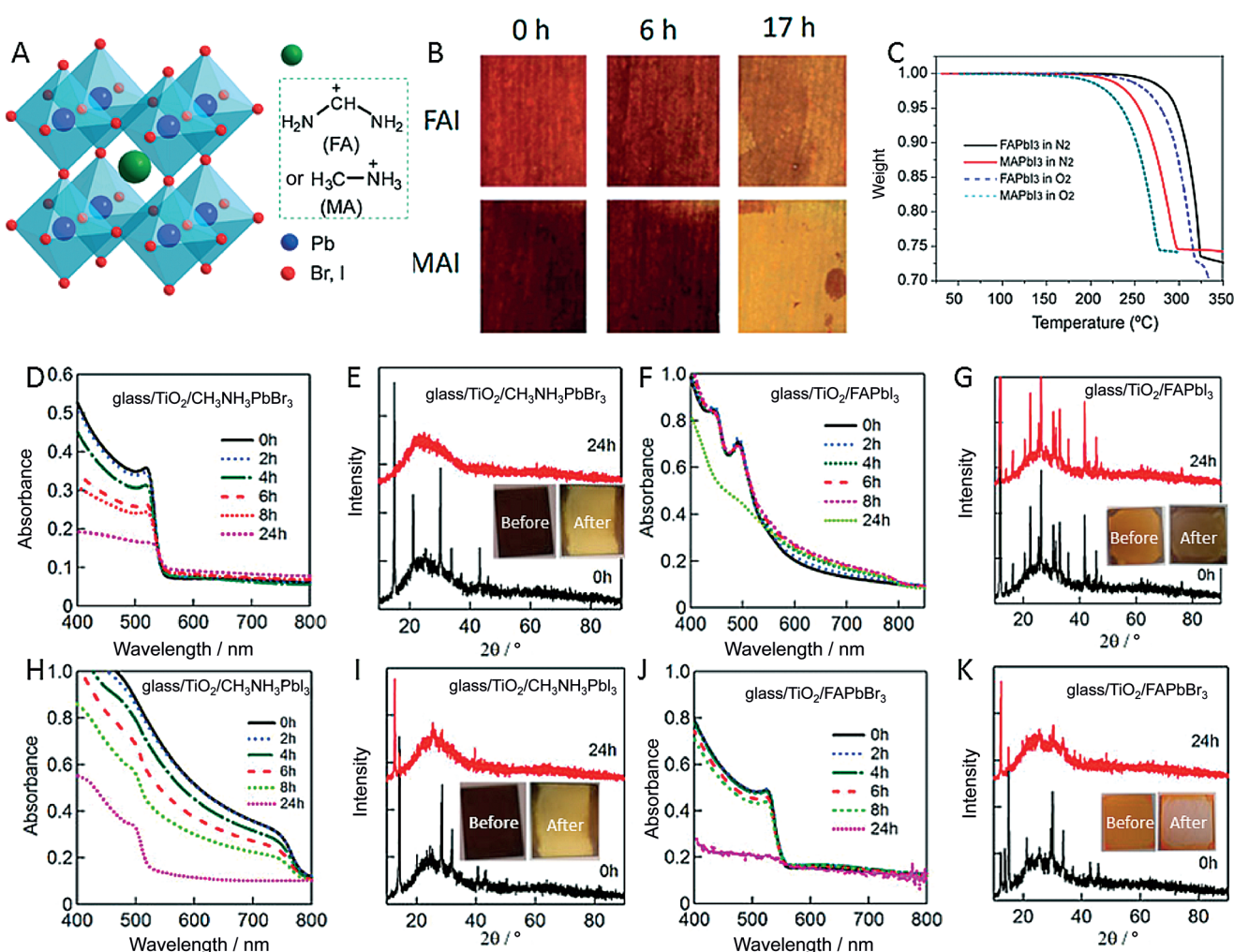


Figure 1. A) Perovskite structure. B) The color change of perovskite made by MAI and FAI under 120 °C in air with relative humidity 50%.^[97] C) TGA curves of MAPbI₃ and FAPbI₃ in nitrogen or oxygen. D), H), F), and J) light absorbance value for MAPbBr₃, MAPbI₃, FAPbI₃, and FAPbBr₃ on TiO₂ substrate under UV/Vis illumination for 24 h; E), G), I), and K) XRD patterns for MAPbBr₃, MAPbI₃, FAPbI₃, and FAPbBr₃ on TiO₂ substrate before and after UV/Vis illumination for 24 h.^[104]

confirmed to form a 3D perovskite with a lower band gap of about 1.47 eV.^[91–93] The organic cation was considered to not take part in determining the band structure, but works to fulfill charge neutrality within the lattice.^[94] However, its size is vital. The size of the organic cation can cause the entire network to enlarge or be compressed. Therefore, both the stability and performance could be expected to improve simultaneously. Park et al. demonstrated FAPbI₃ perovskite has a good thermal stability at a temperature of 150 °C for 25 min.^[95] Zhao et al. also showed a good thermal stability of the FAPbI₃ perovskite at 160 °C for 80 minutes^[96] from a new precursor of HPbI₃ to replace PbI₂ for synthesis of FAPbI₃. Using a chemical vapor deposition method to fabricate FAPbI₃ and MAPbI₃ thin films, the FAPbI₃ is more stable than the MAPbI₃ at 120 °C in air with relative humidity 50 %. The MAPbI₃ thin film decomposed substantially in 17 h while, under the same conditions, FAPbI₃ maintained a similar color to the pristine sample (Figure 1 B).^[97] The improvement of thermal stability may be attributed to the more-stable cubic phase of FAPbI₃ compared to tetragonal phase of MAPbI₃.

Moreover, Seok et al. demonstrated FA⁺ can also protect Sn²⁺ from oxidation to Sn⁴⁺ and showed that FASnI₃ did not exhibit an efficiency loss when encapsulated and stored in the dark under a relative humidity about 25 % and temperature about 25 °C for more than 100 days.^[98] The thermal stability of completely FA⁺ substituted perovskite was also enhanced in oxygen. Jin et al. compared the thermal degradation of MAPbI₃ and FAPbI₃ in nitrogen and oxygen, respectively (Figure 1 C), and suggested that FAPbI₃ is the more thermally stable in nitrogen and oxygen.^[99] Beyond electrostatics, in fact, the interaction between the A cations and the halides in the perovskite structure mainly occur through hydrogen bonding between the acidic MA or FA hydrogen atoms and the perovskite iodides. Furthermore, regardless of the cation size, the tetragonal-to-quasi cubic structural evolution when moving from MA⁺ to FA⁺ is due to enhanced hydrogen bonding to the inorganic matrix and thus alters the covalent/ionic character of Pb–I bonds.^[92] Therefore, the greater thermal stability of FAPbI₃ in nitrogen and oxygen may originate from the enhanced hydrogen bonding between FA⁺

and I^- since the FA^+ has a higher propensity to form hydrogen bonds.^[92,100] This propensity may be due to the statistically enhanced probability of forming hydrogen bonds because of the increased number of protons in FA^+ than in MA^+ . Moreover, replacing MA with FA can reduce the extent of Sn oxidation in $FASnI_3$ perovskite because FA forms a stronger hydrogen bond with H_2O , leading to a partial expansion of the perovskite network.^[101]

The light stability in humidity of $FAPbI_3$ is also improved compared to $MAPbI_3$.^[102] The main mechanism of the poor light stability of $MAPbI_3$ is that MA^+ will release protons under light illumination, which makes the protons and the I^- combine to generate HI.^[27,38] For $FAPbI_3$, the main reason for the stability under light illumination is that it is difficult for FA^+ to release protons. This is mainly because the FA^+ is stabilized by the resonance characteristics of the C–N bonds.^[100,103] Ito and co-workers investigated perovskite light stability under UV/Vis light illumination for 24 h (Figure 1D–K). The light absorbance of $FAPbI_3$ and $FAPbBr_3$ can remain stable under light illumination for 8 h

while light absorbance dropped quickly after light illumination for $MAPbI_3$ and $MAPbBr_3$.^[104] The corresponding XRD patterns and inserted photos also match well with the absorption.^[103]

Etgar and co-workers^[105] described a much more stable perovskite in which there was partial substitution of FA^+ by MA^+ . $MAPbI_3$ and $FAPbI_3$ perovskite both actually showed very poor thermal stability in hole-conductor-free perovskite solar cells. A $MAPbI_3$ perovskite thin film with the best surface coverage is formed when the annealing temperature is 100 °C (Figures 2A,D,G). However, at a temperature of 175 °C, the film changed to a honeycombed structure and the surface coverage is worse while at a temperature of 230 °C it becomes yellow, which suggests $MAPbI_3$ gradually decomposes into PbI_2 , indicating a serious thermal instability. The mixed perovskite with partial substitution of MA^+ by FA^+ showed no significant change in surface coverage under annealing temperatures of 100 °C, 175 °C, and 230 °C, indicating that the partial substitution of MA^+ is a way to improve perovskite thermal stability (Figure 2B,E,H). However, it is

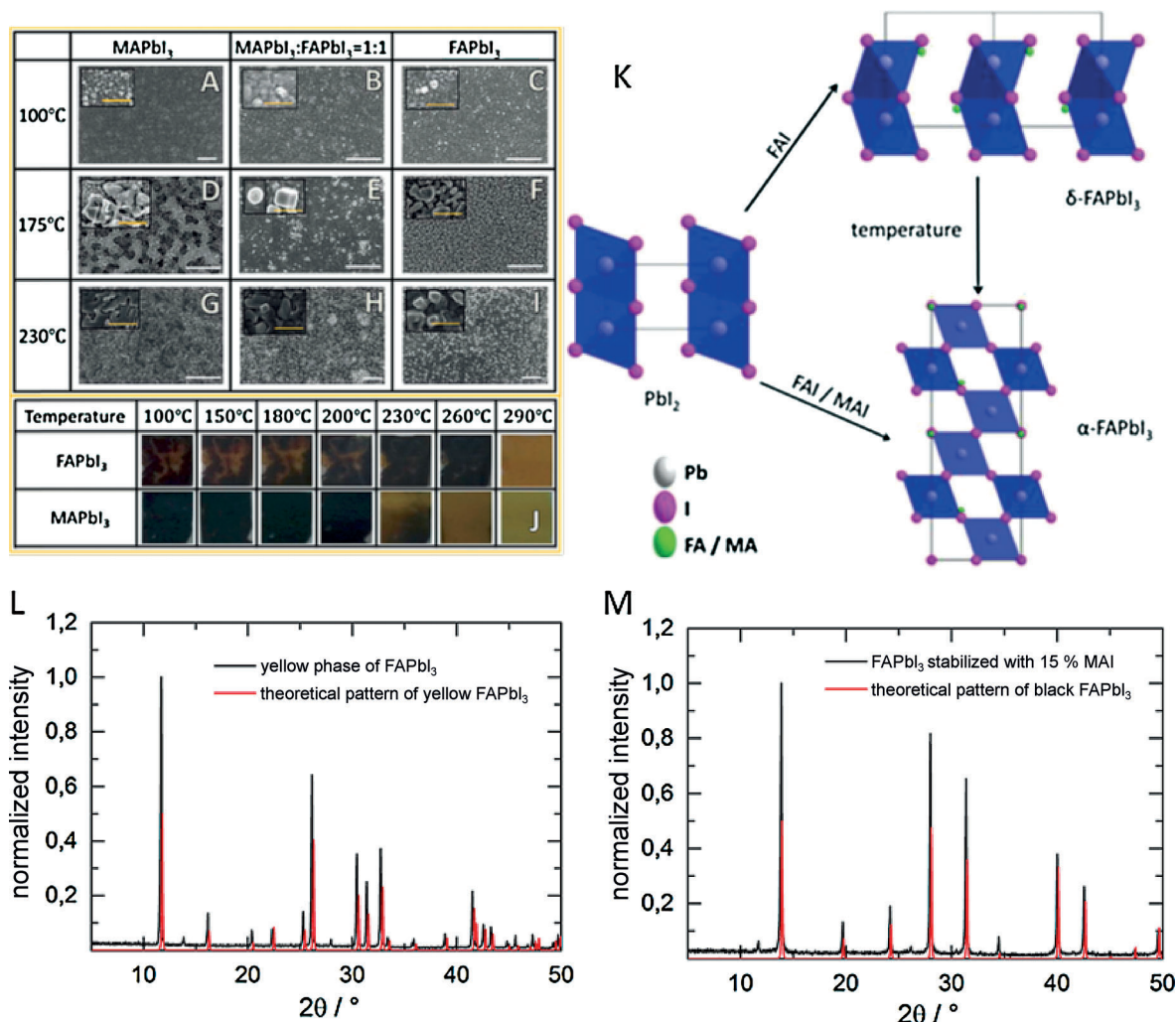


Figure 2. SEM images of perovskite thin films prepared at different annealing temperatures. A), D), and G) $MAPbI_3$ annealing at 100 °C, 175 °C, and 230 °C; B), E), and H) $MAPbI_3/FAPbI_3$ in 1:1 annealing at 100 °C, 175 °C, and 230 °C; C), F), and I) $FAPbI_3$ annealing at 100 °C, 175 °C, and 230 °C. J) $FAPbI_3$ and $MAPbI_3$ on substrates, prepared at different annealing temperatures.^[105] K) The transformation of $FAPbI_3$ with different crystal phases. XRD curves of yellow phase of $FAPbI_3$ (L) and $FAPbI_3$ with 15 % MAI (M). Red line is the theoretical XRD curve.^[100]

clear that the surface coverage of the FAPbI₃ perovskite changes little with gradually increasing the temperature from 100 °C to 175 °C and 230 °C, showing a much better stability than MAPbI₃ (Figure 2C,F,I). Although with further increasing the temperature to 290 °C the FAPbI₃ perovskite decomposes into yellow PbI₂ (Figure 2J), however, FAPbI₃ is more stable than the MAPbI₃ perovskite, which may totally lose activity at 260 °C. Moreover, it is also beneficial to form a FAPbI₃ crystal with an α phase at low temperature with the partial substitution of FA⁺ by MA⁺. The transformation of FAPbI₃ with different crystal phases is presented in Figure 2K. The XRD curve of FAPbI₃ matches well with theoretical pattern of yellow and black FAPbI₃ (Figure 2L,M), but the perovskite can be stabilized with 15% CH₃NH₃I(MAI).^[100] This change may be achieved by enhancing the I–H hydrogen bond between the cations and inorganic ligands, or by enhancing the Madelung energy of the structure, which improved the decomposed energy of this perovskite crystal.^[106,107]

2.2. Effect of Cs Cations

Cesium lead halides (e.g., CsPbI₃) perovskite solar cells have recently been intensively investigated as a result of the appropriate ionic radius of Cs⁺ for the perovskite 3D structure and resulting improved stability. Snaith et al. first demonstrated that cubic CsPbI₃ perovskite can be formed over 310 °C and it is very stable at low temperature for 200 days when it's stored in inert air, indicating it is a significantly more thermally stable material.^[108] Moreover, a much more stable perovskite material CsPbI₂Br was fabricated by partial substitution of I[−] in CsPbI₃ with Br[−]. Snaith et al. compared the stability of CsPbI₂Br and MAPbI₂Br for 300 mins under heating at 85 °C in relative humidity of 20–25 %, as depicted in Figure 3. A dramatically decreased absorption value indicates MAPbI₂Br is not stable when heating at 85 °C in relative humidity of 20–25 % (Figure 3A).^[109] However, CsPbI₂Br is stable showing no change in absorption under same conditions (Figure 3B). The XRD patterns also confirmed this (Figure 3C,D) with CsPbI₂Br

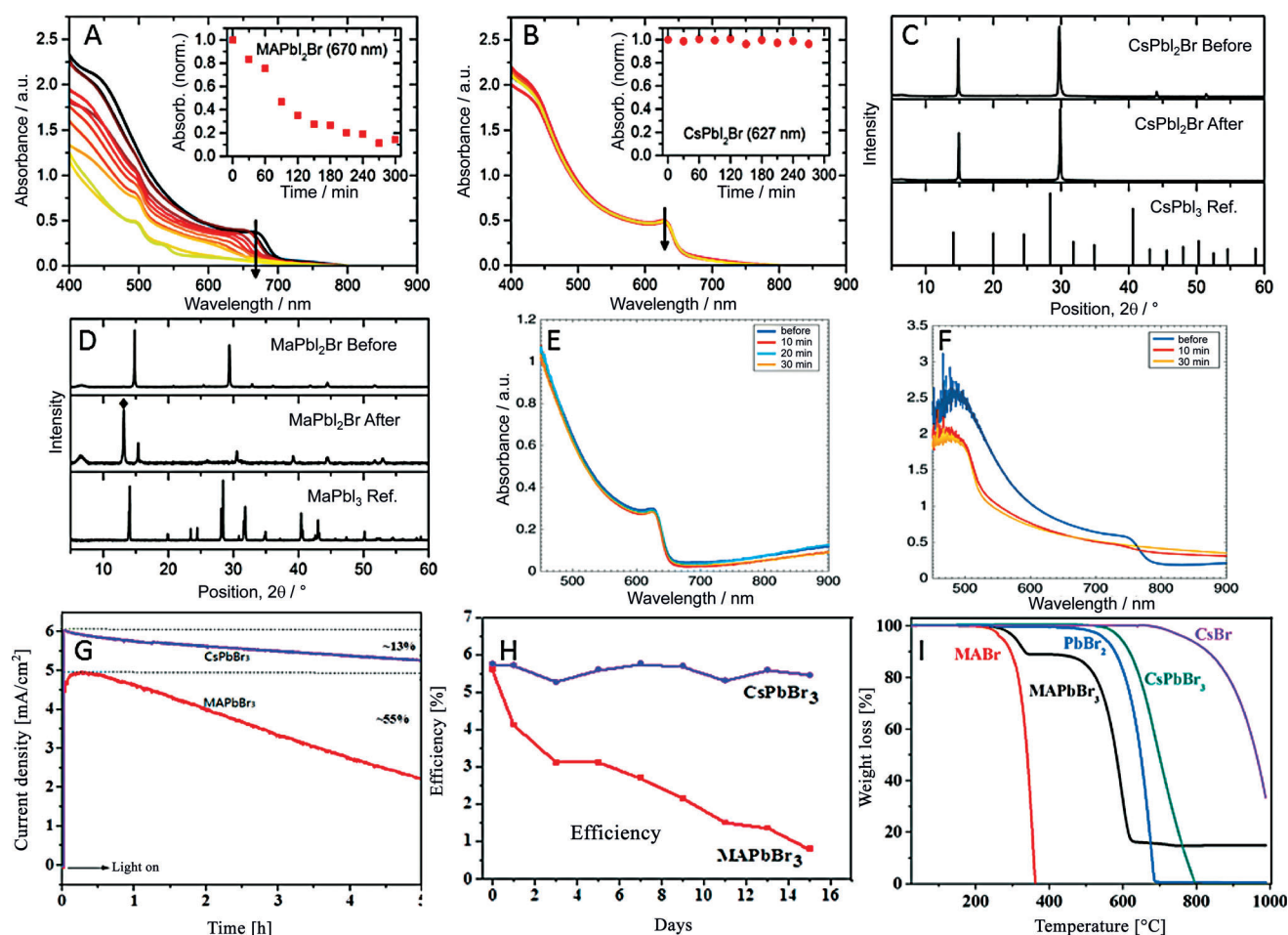


Figure 3. Absorbance of MAPbI₂Br (A) and CsPbI₂Br (B) heated at 85 °C for different times in a relative humidity of 20–25 %. Inset: The normalized absorbance value at 670 nm for MAPbI₂Br and at 627 nm for CsPbI₂Br. XRD patterns for CsPbI₂Br (C) and MAPbI₂Br (D) after heating at 85 °C in relative humidity of 20–25 % for 270 min.^[109] Absorbance of CsPbI₂Br (E) and MAPbI₂Br (F) heated for different times at 180 °C.^[111] G) Stability in current density of MAPbBr₃ and CsPbBr₃ solar cells under 100 mW/cm² AM 1.5 illumination. H) Stability in efficiency of MAPbBr₃ and CsPbBr₃ solar cells exposed into ambient air under relative humidity of 60%–70%. I) TGA curves of MAPbBr₃, CsPbBr₃, and their components.^[112]

showing little change while a new peak of PbI_2 appeared in MAPbI_2Br curves accompanied by weaker perovskite diffraction. Similar work has been conducted by McGehee et al. and Huang et al. with similar results, further confirming the stability of CsPbI_2Br and CsPbIBr_2 Perovskite, respectively.^[110,111] As shown in Figure 3 E,F, the absorbance value dropped for MAPbI_2Br but was stable for CsPbI_2Br after heating at 180 °C for 30 mins. Moreover, the total substitution of I^- by Br^- (CsPbBr_3) can further improve the stability of the perovskite and its related perovskite solar cells under full light illumination (Figure 3 G) and exposure to ambient air under relative humidity of 60%–70% (Figure 3 H). The main reason for the enhanced stability is the more thermally stable component CsBr (Figure 3 I). The decomposition of MAPbBr_3 was dominated by two steps: the first step onset at around 220 °C corresponds to the loss of MABr ; the second step onset at about 450 °C corresponds to the loss of PbBr_2 . However, from the TGA analysis (Figure 3 I), the CsBr has a higher decomposition temperature than PbBr_2 , and much higher than MABr , which inversely contributes to the improvement of CsPbBr_3 .^[112]

The t value is an empirical index for predicting stable crystal structures of perovskite materials. The t value of Cs^+ incorporated $\text{FA}_{1-x}\text{Cs}_x\text{PbI}_3$ perovskite was systematically investigated by Zhu and co-workers.^[113] They found that this perovskite $\text{FA}_{0.85}\text{Cs}_{0.15}\text{PbI}_3$ with 15% Cs^+ incorporation has a t value of 0.9 with a cubic and α phase. FAPbI_3 and $\text{FA}_{0.85}\text{Cs}_{0.15}\text{PbI}_3$ thin films were exposed to a humid environment for 18 days, the absorbance value of FAPbI_3 thin films decreased very fast while that of $\text{FA}_{0.85}\text{Cs}_{0.15}\text{PbI}_3$ thin films remained stable (Figures 4 A,B). Accordingly, the performance of $\text{FA}_{0.85}\text{Cs}_{0.15}\text{PbI}_3$ and FAPbI_3 perovskite solar cells follows similar trends as the absorbance spectra under the same conditions (Figure 4 C,D). The PCE of the $\text{FA}_{0.85}\text{Cs}_{0.15}\text{PbI}_3$ solar cell showed almost no change while that of FAPbI_3 decreased to about half the initial value when exposed to humid air for 400 h (Figure 4 E). From Figure 4 F, the improved stability of the $\text{FA}_{0.85}\text{Cs}_{0.15}\text{PbI}_3$ perovskite can clearly be seen.^[114] Moreover, Grätzel et al. found that a 20% incorporation of Cs^+ to give the $\text{FA}_{0.8}\text{Cs}_{0.2}\text{PbI}_{2.84}\text{Br}_{0.16}$ perovskite can also improve the stability compared to FAPbI_3 perovskite on exposure to a humid environment in 1000 h (Figure 4 G).^[113]

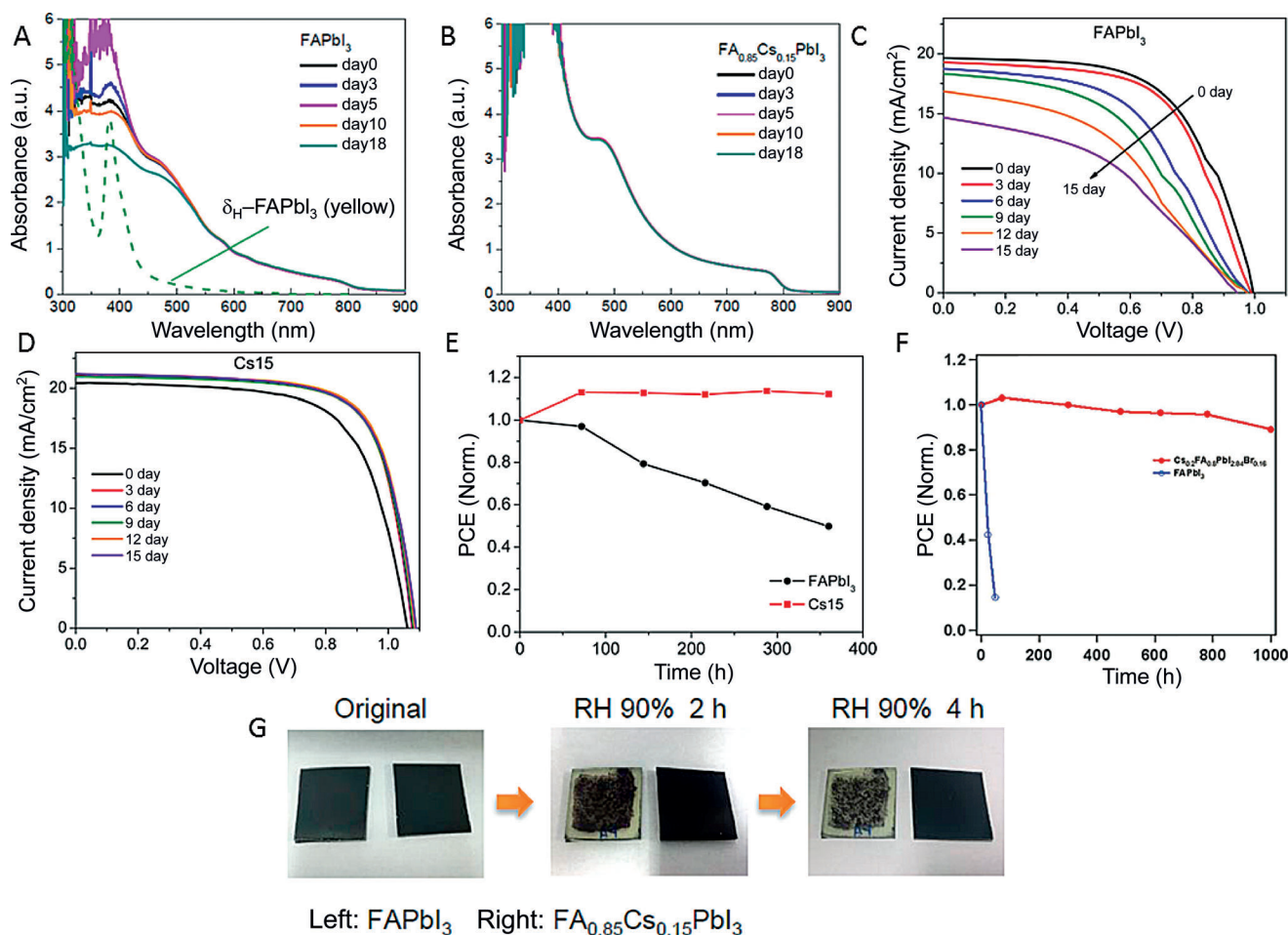


Figure 4. Absorbance of FAPbI_3 (A) and $\text{FA}_{0.85}\text{Cs}_{0.15}\text{PbI}_3$ (B) thin films exposed to the air. J - V curves of devices based on FAPbI_3 (C) and $\text{FA}_{0.85}\text{Cs}_{0.15}\text{PbI}_3$ (D) thin films exposed to the air for 15 days. E) Normalized PCE of FAPbI_3 and $\text{FA}_{0.85}\text{Cs}_{0.15}\text{PbI}_3$ based devices in humid conditions.^[114] F) Stability of FAPbI_3 and $\text{FA}_{0.8}\text{Cs}_{0.2}\text{PbI}_{2.84}\text{Br}_{0.16}$ exposed into humid air for 1000 h. G) Comparison of degradation of FAPbI_3 and $\text{FA}_{0.85}\text{Cs}_{0.15}\text{PbI}_3$ in humid conditions for 4 h.^[113]



Recently, a partial substitution of FA^+ by Cs^+ in FAPbI_3 perovskite was found to substantially improve photo- and moisture stability along with photovoltaic performance. When FAPbI_3 is doped with different levels of Cs^+ , the FAPbI_3 crystal phase will be different and there will be changes in the absorption and XRD patterns (Figures 5 A,B). When 10% of FA^+ is replaced by Cs^+ , the stability of the perovskite thin films under light illumination and moisture are significantly improved. FAPbI_3 and $\text{FA}_{0.9}\text{Cs}_{0.1}\text{PbI}_3$ gave similar absorptions for the first 8 h of illumination monitored at 630 nm under the light illumination in 100 mW cm^{-2} ,

FAPbI_3 and $\text{FA}_{0.9}\text{Cs}_{0.1}\text{PbI}_3$ perovskites under light illumination (100 mW cm^{-2}) and ambient conditions ($\text{RH} < 40\%$) for 30 min, the normalized PCE of $\text{FA}_{0.9}\text{Cs}_{0.1}\text{PbI}_3$ perovskite decreased 70% whereas the pristine perovskite decreased 80% (Figure 5D). Furthermore, trap density is reduced by one order of magnitude upon incorporation of Cs^+ , which is responsible for the increased open-circuit voltage and fill factor, eventually leading to enhancement of average PCE from 14.9% to 16.5%.^[102]

Moreover, the effect on stability of the presence of Cs^+ in triple cation perovskite $\text{Cs}_x(\text{MA}_{0.17}\text{FA}_{0.83})_{(100-x)}\text{Pb}(\text{I}_{0.83}\text{Br}_{0.17})_3$

(abbreviated as Cs_xM) has been systematically investigated by Grätzel et al., and found that this triple cation perovskite is more stable under high temperature and illumination.^[115] The perovskite without Cs^+ [$(\text{MA}_{0.17}\text{FA}_{0.83})\text{Pb}(\text{I}_{0.83}\text{Br}_{0.17})_3$] is not stable in dry air at 130°C for 3 h and develops a very faded film surface and reduced light absorbance (Figure 6A), however, incorporation of 10% Cs^+ into the perovskite can remarkably improve its thermal stability (Figure 6B). Moreover, perovskite containing 10% Cs^+ without annealing has similar XRD diffraction peaks to the annealed perovskite and its surface color and absorbance value is similar to the annealed perovskite (Figure 6C). Interestingly a perovskite crystal without Cs^+ doping cannot be formed by spin coating at 18°C in spite of being annealed at 100°C , whereas after doping with 10% of Cs a perovskite crystal can be formed at the same low temperature (Figure 6D), indicating Cs^+ has a significant effect on the transformation of the perovskite from the δ phase to the α phase. Moreover, the Cs^+ doped

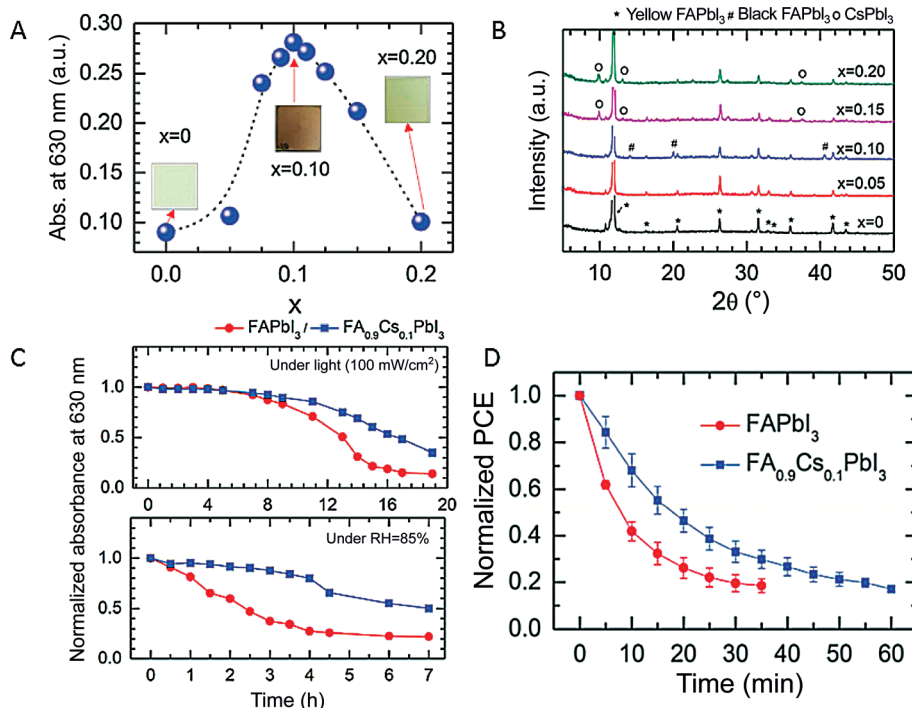


Figure 5. A) Absorbance at 630 nm with different Cs contents. B) XRD patterns of perovskite $\text{FA}_{1-x}\text{Cs}_x\text{PbI}_3$ with different Cs contents. C) Normalized absorbance at 630 nm for FAPbI_3 (red solid circle) and $\text{FA}_{0.9}\text{Cs}_{0.1}\text{PbI}_3$ (blue square) under illumination (100 mW cm^{-2}) and relative humidity 85%. D) Decreased of the normalized PCE for FAPbI_3 (red solid circle) and $\text{FA}_{0.9}\text{Cs}_{0.1}\text{PbI}_3$ (blue square) during illumination (100 mW cm^{-2}) under relative humidity of 85%.^[102]

however, the absorption of FAPbI_3 decreased rapidly while the absorption value of $\text{FA}_{0.9}\text{Cs}_{0.1}\text{PbI}_3$ decreased more slowly than that of FAPbI_3 with further illumination (Figure 5C). Moreover, the absorption of FAPbI_3 decreased dramatically compared to that of $\text{FA}_{0.9}\text{Cs}_{0.1}\text{PbI}_3$ in a relative humidity of 85%. The improved stability of the $\text{FA}_{0.9}\text{Cs}_{0.1}\text{PbI}_3$ perovskite is attributed to the enhanced interaction between FA^+ and I^- due to the contraction of the cubo-octahedral cavity by incorporation of Cs^+ . Moreover, in a humid environment FAPbI_3 is easily converted from the black phase to the yellow phase or there is an accelerated dissociation of FA^+ to ammonia and *sym*-triazine^[9] whereas $\text{FA}_{0.9}\text{Cs}_{0.1}\text{PbI}_3$ is expected to be more stable because incorporation of 10% Cs stabilizes the black FAPbI_3 phase at relatively low temperature and Cs^+ hardly undergoes such a dissociation. They have also investigated the stability of non-encapsulated

device is stable for over 250 h at room temperature under constant illumination while for the device without Cs^+ doping the PCE decreased dramatically (Figure 6E). Surprisingly, the device with 5% Cs^+ doping has a stable PCE of 21.1%,^[115] which is the current record (Figure 6F).

2.3. Substitutions of Aliphatic or Aromatic Alkylammonium Cations

MA^+ , FA^+ , and Cs^+ are widely investigated cations to substitute each other in 3D perovskite structures owing to their suitable radius in the range of r . If the small MA^+ , FA^+ , or Cs^+ is replaced by a much larger organic primary ammonium cation, the 3D perovskite would move to a 2D layered structure as a result of steric effects. Very recently,

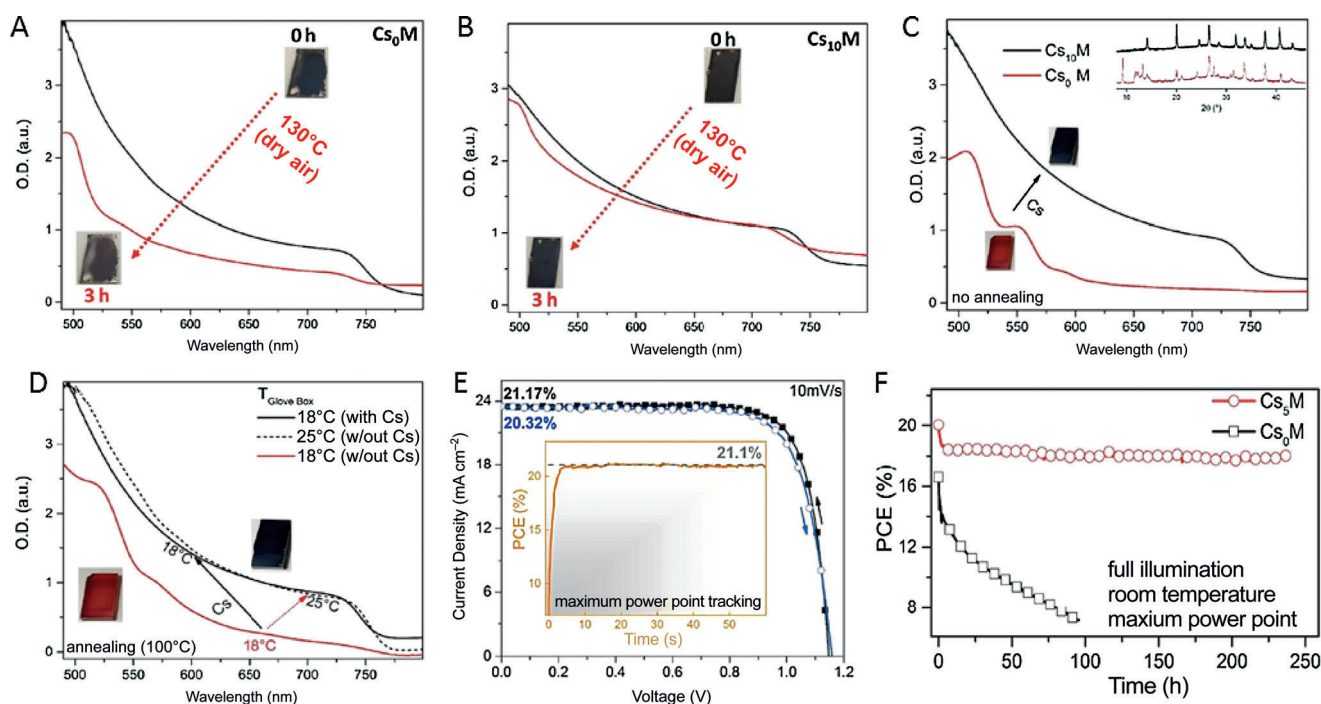


Figure 6. A), B) UV/Vis absorption of Cs_0M and Cs_{10}M thin films annealed at 130°C in dry air for 3 h, and the change of their corresponding images. C) Absorption curves and images of no annealed Cs_0M thin film (red line), and Cs_{10}M thin film (black line). Insert: XRD patterns for Cs_0M (red line) and Cs_{10}M (black line). D) No perovskite phase formed in UV/Vis curve for Cs_0M in spin coating at 18°C (red line). But a clearly perovskite phase formed for Cs_0M spin coating at 25°C (dashed line) and Cs_{10}M spin coating at 18°C (black line). The insert images are their thin films annealed at 100°C for Cs_0M spin coating at 18°C (red), 25°C (black) or for Cs_{10}M spin coating at 18°C (black). E) J - V curves of Cs_5M perovskite solar cell under forward and reverse scan. The inset shows the maximum power point tracking for 60 s in forward scan. F) The maximum power point of perovskite solar cells based on Cs_5M (red curve, circles) and Cs_0M (black curve, squares) in a nitrogen atmosphere at room temperature and constant light illumination for 250 h.^[115]

layered perovskites have attracted much attention owing to their moisture stability. 2D perovskites with layered structure are conceptually derived from the 3D AMX_3 perovskite structure, in which the A and X ions within the planes would be cut into halves. The general formula is $(\text{A})_2(\text{MA})_{n-1}\text{MX}_{3n+1}$ (n is an integer), where A is a primary aliphatic or aromatic alkylammonium cation, M is a divalent metal ions, and X is a halide anion. They are analogous to the simplest inorganic Ruddlesden–Popper phase of the K_2NiF_4 crystal.^[116] The large alkylammonium cations are inserted between interdigitated bilayers and confined by inorganic layers of corner-sharing $[\text{MX}_6]^{4-}$ octahedra.^[117] To maintain the structural integrity, the layers are stacked together by a combination of Coulombic and hydrophobic forces.

Karunadasa et al. for the first time demonstrated a 2D layered perovskite $(\text{PEA})_2(\text{MA})_2[\text{Pb}_3\text{I}_{10}]$ by integrating $\text{C}_6\text{H}_5(\text{CH}_2)_2\text{NH}_3^+$ (PEA^+) into a 3D MAPbI_3 perovskite.^[118] The crystal structures of MAPbI_3 and $(\text{PEA})_2(\text{MA})_2[\text{Pb}_3\text{I}_{10}]$ are shown in Figure 7A. High-quality $(\text{PEA})_2(\text{MA})_2[\text{Pb}_3\text{I}_{10}]$ films can easily be achieved and high-temperature annealing is not required for device fabrication. To compare their moisture stability, three perovskite films $[(\text{PEA})_2(\text{MA})_2[\text{Pb}_3\text{I}_{10}]]$, MAPbI_3 from a precursor solution of PbI_2 and MAI in 1:1, and MAPbI_3 film from a precursor solution of PbCl_2 and MAI in 1:3 have been exposed to 52 % relative humidity. After exposure to humidity for 46 days, the $(\text{PEA})_2(\text{MA})_2[\text{Pb}_3\text{I}_{10}]$ perovskite film gave the same XRD

pattern as before the exposure (Figure 7B), suggesting a good stability to moisture. The MAPbI_3 perovskite films, however, showed a new diffraction peak of PbI_2 in just 4 days, which gradually got much stronger (Figures 7C,D). The comparison of absorption between MAPbI_3 and $(\text{PEA})_2(\text{MA})_2[\text{Pb}_3\text{I}_{10}]$ can further confirm the improvement of stability (Figure 7E,F). The property of enhanced moisture stability in this structure may be attributed to the layers preventing the intrusion of water molecules. However, decreasing the dimensionality of the inorganic components from the 3D structure causes an increase in the band gap to an estimated value of approximately 2.1 eV for $(\text{PEA})_2(\text{MA})_2[\text{Pb}_3\text{I}_{10}]$, leading to lower device performance (4.73 %; Figure 7G).

Sargent et al. systematically investigated PEA-based layered perovskite structures by continuously tuning the dimensionality of metal halide perovskite compounds by mixing stoichiometric quantities of PbI_2 , MAI, and PEA to yield compounds with different layer (n) values in the series $(\text{PEA})_2(\text{MA})_{n-1}\text{Pb}_n\text{I}_{3n+1}$ with $n = 6, 10, 40, 60$, and ∞ , where $n = \infty$ corresponds to the cubic 3D perovskite (MAPbI_3) and other n values describe 2D ($n = 1$) or quasi-2D ($n > 1$) perovskite structures (Figure 8A).^[119] An energy of 0.36 eV is required to remove PEA from the layered perovskite structure, which is higher than that for MAI. This change significantly reduced the desorption rate by six orders of magnitude and slowed film decomposition 1000-fold. The material stability was investigated as a function of dimen-

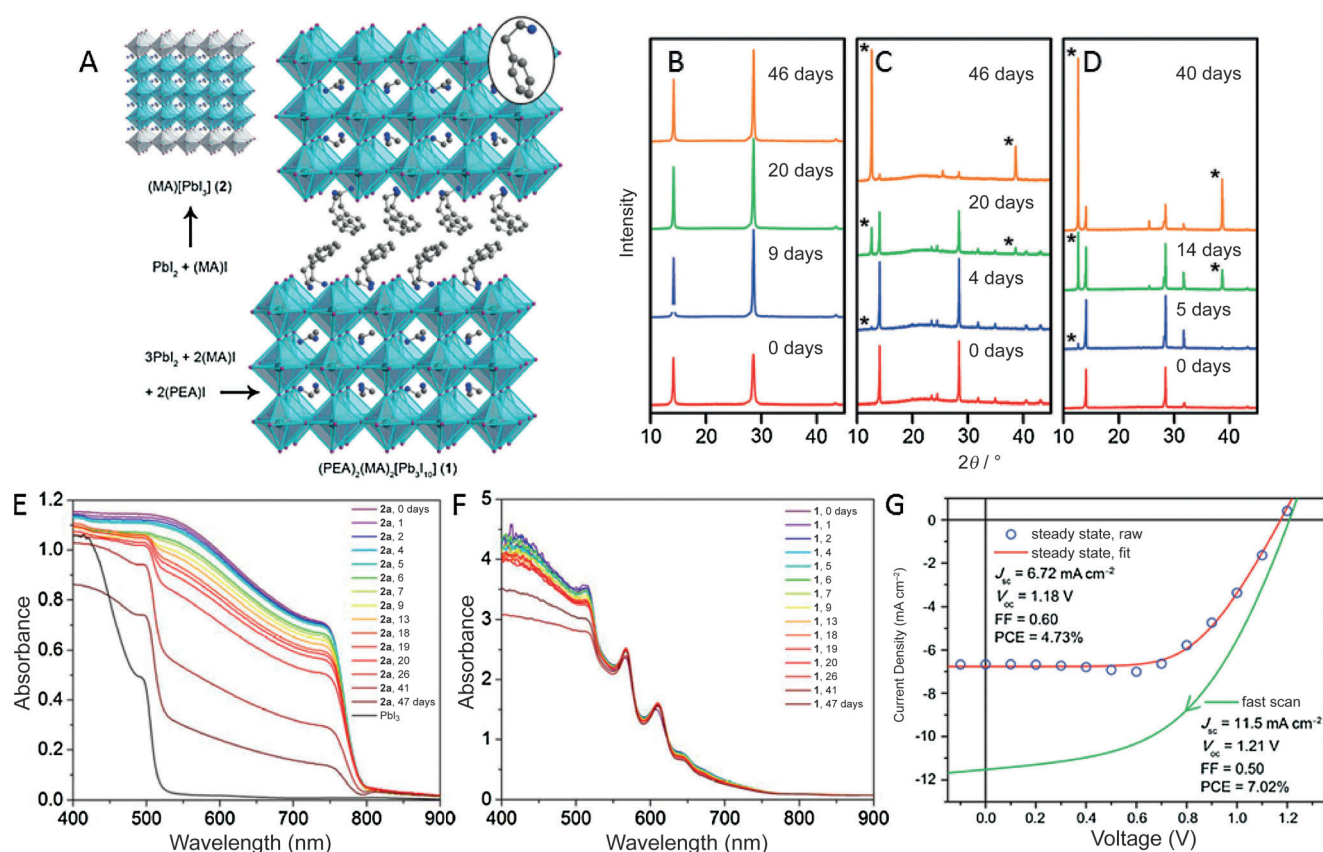


Figure 7. A) Crystal structure of 3D perovskite MAPbI₃, 2D perovskite (PEA)₂(MA)₂[Pb₃I₁₀], and their simple synthesis process. Inset: structure of PEA⁺. XRD patterns after different numbers of days: B) (PEA)₂(MA)₂[Pb₃I₁₀], C) MAPbI₃ formed from PbI₂ with a poor morphology, and D) PbI₂ with better morphology. E), F) Absorption spectra of films of MAPbI₃ and (PEA)₂(MA)₂[Pb₃I₁₀], respectively, upon exposure to a relative humidity of 52%. G) *J*-*V* curves for the devices employing (PEA)₂(MA)₂[Pb₃I₁₀].^[118]

sionality, by absorption, XRD, and transient photoluminescence (PL) decay (Figure 8B,C,D). After two months, the absorbance of 3D perovskite films at wavelengths longer than 500 nm is significantly suppressed and a new peak at 12.42° of PbI₂ emerges in the XRD pattern for 3D perovskite films while the quasi-2D perovskites (*n* = 10, 40, 60) exhibit significantly improved stability with no or only slight variation in the absorbance and only a very weak PbI₂ reflection appears in the *n* = 60 and *n* = 40 perovskite films, indicating a significant improvement of stability compared to 3D perovskite. Their PL decay measurements provide further support of enhanced stability for quasi-2D perovskites. Dramatic changes are observed in the PL decay traces for the 3D perovskite after 10 days storage in air whereas there was no observable variation in the charge-carrier lifetime of quasi-2D (*n* = 40, 60) perovskites. Moreover, the device stability was also remarkably improved (Figures 8E–I). The 3D perovskite devices degraded over 8 weeks from initial 16.6% to less than 3% when stored in N₂, whereas the quasi-2D perovskites based devices declined to 11.3% (*n* = 60) and 13.1% (*n* = 40) after 60 days under a low-humidity atmosphere. In analogous studies under 55% humidity in air, the 3D perovskite lost the majority of its performance, while the *n* = 60 and *n* = 40 devices decreased to about 13% in each case. It was concluded that the very low formation energy of

3D perovskites is responsible for their low stability while much higher formation energies are needed in quasi-2D perovskites as a result of the appreciable van der Waals forces, which confer improved stability (Figure 8J). The additional organic cations with larger radius can actually protect the perovskite structure as a capping layer in quasi-2D perovskite.

Kanatzidis et al. reported the fabrication and properties of the 2D lead iodide perovskite (CH₃(CH₂)₃NH₃)₂(MA)_{*n*-1}Pb_{*n*}I_{3*n*+1} (*n* = 1–4) thin films employing the large alkylammonium ion CH₃(CH₂)₃NH₃⁺ (BA⁺).^[120] The 2D perovskite films are formed in a self-assembly fashion with preferentially oriented growth perpendicular to the substrate (Figure 9A–J). As expected, the (BA)₂(MA)_{*n*-1}Pb_{*n*}I_{3*n*+1} perovskites are moisture resistance compared to their 3D MAPbI₃ analogues. For example, a film of (BA)₂(MA)₂Pb₃I₁₀ (*n* = 3) was investigated by XRD and the peaks remained unchanged after 2 months exposure under a 40% humid condition (Figure 9A), which shows its better stability for devices (Figure 9B). Moreover, the color of these 2D perovskite films remained the same as when they were fabricated. However, a film of MAPbI₃ gradually decomposed to yellow PbI₂ after a short time in the same moist atmosphere (Figure 9C). It was proposed that the moisture-resistance of the (BA)₂(MA)_{*n*-1}Pb_{*n*}I_{3*n*+1} perovskites

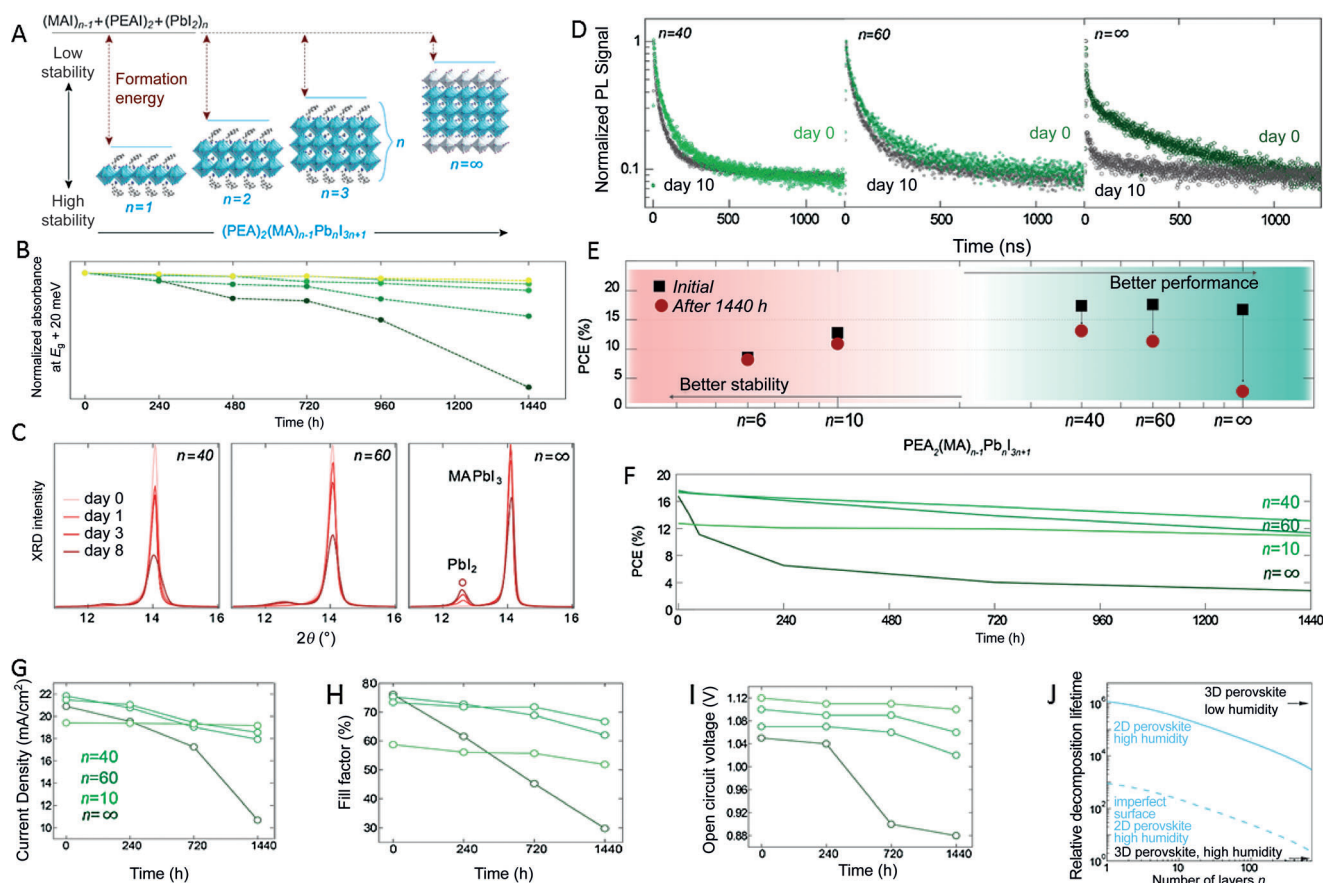


Figure 8. A) Unit cell structure of $(C_8H_9NH_3)_2(MA)_{n-1}PbI_{3n+1}$ perovskites with different n values. B) Normalized absorption spectra, C) XRD patterns, and D) PL decay data of MAPbI₃ and quasi-2D perovskites before and after 10 days storage. E) PCE of devices based on MAPbI₃ and quasi-2D perovskites before and after 1440 h storage. Stability of F) PCE, G) J_{sc} , H) FF, and I) V_{oc} of perovskites with different n values. J) DFT simulation formation energy of perovskites with different n values in different atmospheres.^[119]

may result from the hydrophobicity of the long BA⁺ chain and the highly oriented and dense nature of the perovskite films, which prevents direct contact of water molecules with the perovskite.

Generally, layered 2D perovskites tend to crystallize in a direction parallel to the substrate.^[118,120,121] As a consequence, the charge transport could be greatly hindered in the directions perpendicular to the substrate. In this case, Koh et al. report the controlled growth of nanostructured mixed-dimensional perovskites, $(IC_2H_4NH_3)_2(MA)_{n-1}PbI_{3n+1}$, by randomizing the crystallizing direction of 2D perovskites to enhance charge transport and extraction (Figure 10A).^[122] The nanostructured perovskite films are grown using a sequential deposition method under ambient conditions. The dimensionality of the perovskite is controlled by the dipping duration (Figure 10B–D), however, the exact number of layers cannot be controlled. The devices were stored under ambient conditions (25 °C, 70–80 % RH) without any encapsulation. The photocurrent density decreases over time while the photovoltage does not change significantly. Finally, the efficiency of the device decreased just 9 % while that of the 3D MAPbI₃ device degraded over 30 % (Figure 10E,F). In addition, a much larger polymeric-ammonium cation (PEIH⁺) was also used to form a moisture-resistant 2D perovskite, which exhibited good stability, offering greater

tunability at the molecular level for optimization of 2D perovskite materials.^[123]

2.4. Substitution of other Larger Ammonium Cations

Some other larger ammonium cations neither incorporate into perovskite cavity because of the large size nor transform the 3D structure into a 2D layered structure. Instead, non-stoichiometric composition solids were created. However, their specific functions make them suitable additives in the formation of perovskite structures, which gives rise to enhanced structural stability.

Guanidinium (GA⁺; C(NH₂)₃⁺) has similar properties to MA⁺ and FA⁺ but has a larger radius (278 pm), and ought to not form a 3D perovskite structure as the sole A-cation.^[124–126] However, Yamashita et al. have theoretically characterized GAPbI₃, which shows better thermodynamic stability, low formation energy, and low band gap when comparing its structural and electronic properties with those of well-established and well-characterized MAPbI₃ and FAPbI₃.^[127] Furthermore, GA⁺ has a zero dipole moment associated with the *D*_{3h} symmetry, which could potentially reduce the experimentally reported hysteresis observed for smaller cations such as MA⁺.



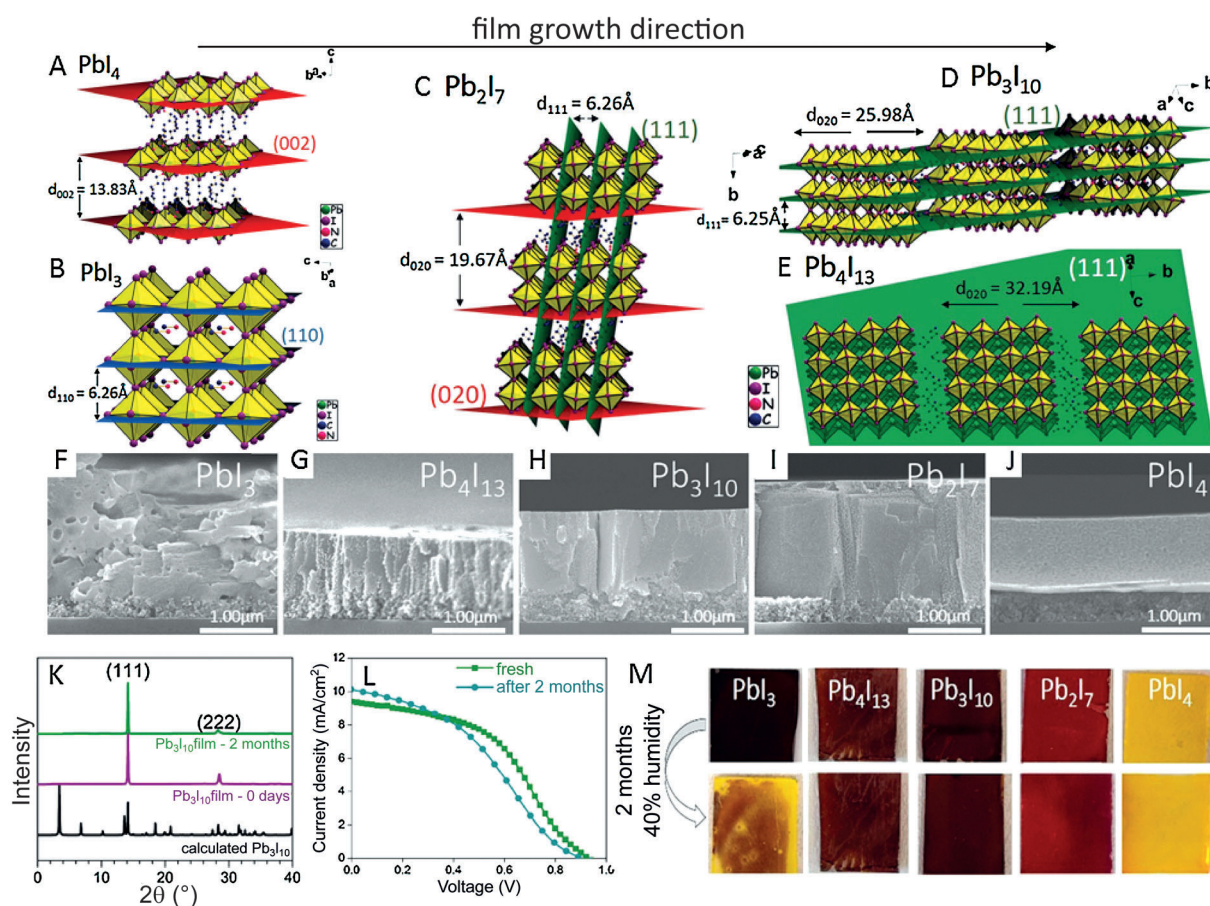


Figure 9. Crystal structure of A) BA_2PbI_4 , B) MAPbI_3 , C) $(\text{BA})_2(\text{MA})\text{Pb}_2\text{I}_7$, D) $(\text{BA})_2(\text{MA})_2\text{Pb}_3\text{I}_{10}$, and E) $(\text{BA})_2(\text{MA})_3\text{Pb}_4\text{I}_{13}$ perovskite. Cross-sectional SEM images of F) MAPbI_3 , G) $(\text{BA})_2(\text{MA})_3\text{Pb}_4\text{I}_{13}$, H) $(\text{BA})_2(\text{MA})_2\text{Pb}_3\text{I}_{10}$, I) $(\text{BA})_2(\text{MA})\text{Pb}_2\text{I}_7$, and J) BA_2PbI_4 on TiO_2 substrates. K) XRD patterns of $(\text{BA})_2(\text{MA})_2\text{Pb}_3\text{I}_{10}$ perovskite film. L) J - V curves of fresh devices and after 2 months storage. M) Images of five perovskite films with different n values before and after exposure to humidity.^[120]

Ethylammonium (EA^+) with one more CH_2 group than MA^+ has a larger radius (230 pm vs. 180 pm), resulting in the band gap increasing from 1.55 eV (MAPbI_3) to 2.2 eV since, like the even larger GA^+ it is hardly able to incorporate into the cavity in the 3D perovskite structure.^[6] However, it also plays a positive role on the morphology (Figure 11 A–C) and stability of the perovskite. Figure 11 D shows the stability of perovskite solar cells based on $\text{MAPbI}_{3-x}\text{Cl}_x$ perovskite with EAI concentrations of 0%, 0.5% and 1% upon storage under Ar atmosphere in the dark. Devices containing 1% EAI perovskite exhibited extremely high stability, retaining approximately 80% of their PCEs (T_{80}) under accelerated heating (65 °C) in a dark N_2 -filled glove box for over 360 h, whereas the reference device (0% EAI) was relatively sensitive to this temperature, with a T_{80} value of only 45 h (Figure 11 D). It was claimed that the improved stability originated from the presence of EAI suppressing the morphological change, and thus decreasing the deterioration in the absorption and crystallinity of the perovskite films.^[128]

Bifunctional ammonium cations,^[129,130] for example, the 4-ammonium butyric acid cation, alanine cation, and β -glycine cation, have been gradually explored in perovskite solar cells because they bring about a retardation of charge recombina-

tion and better controlled crystal growth. Han et al. first reported that 5-aminovaleric acid cations (5-AVA^+) can be used as a template for the preferential crystal growth of MAPbI_3 in the mesoporous oxide host by forming hydrogen bonds between its COOH and NH_3^+ groups and I^- ions from the PbI_6 octahedra.^[74] The COOH group of 5-AVA coordinated with Ti or Zn on the surface of mesoporous TiO_2 or ZnO_2 and the NH_3^+ ions on the terminal of 5-AVA⁺ served as nucleation sites for the formation of the perovskite crystal, as shown in Figure 11 E,F. The resulting perovskite has better surface contact with the TiO_2 surface and a lower defect concentration than MAPbI_3 , resulting in an improved PCE and excellent long-term stability. The cell with 5-AVA⁺ modified perovskite worked stably for more than 1000 h in humid air and under full sunlight (Figure 11 G–J).

Bi et al. have developed a new fluorinated 1,1,1-trifluoroethyl ammonium iodide (FEAI) additive for MAPbI_3 perovskites to enhance the stability to the environment without sacrificing the performance of the devices.^[131] FEAI⁺ has a hydrophilic side and a hydrophobic side (Figure 12 A), which can interact strongly with 3D perovskites and improve their stability as a result of the hydrophobic CF_3 terminal groups covering the surface of the perovskite. To evaluate the

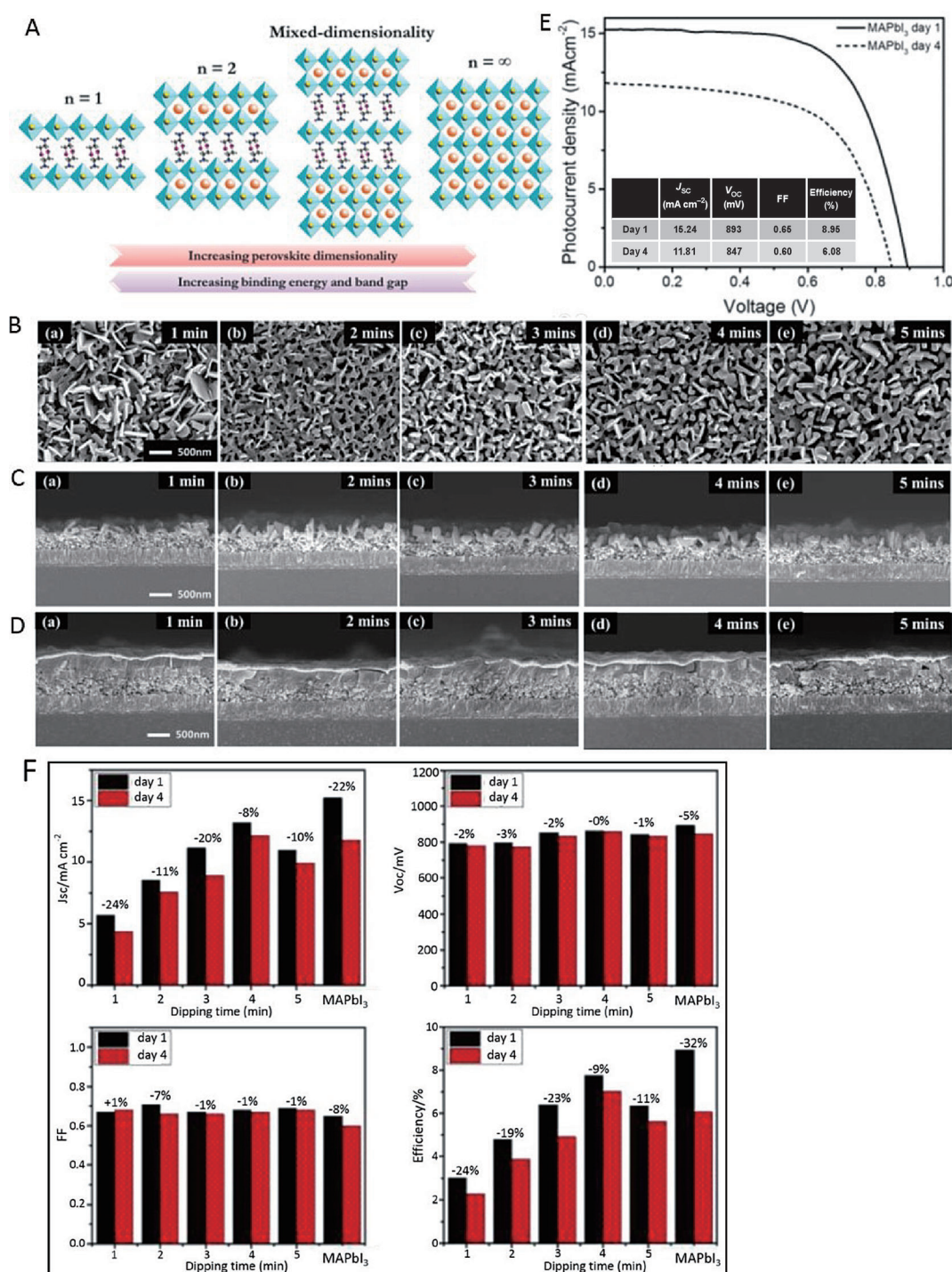


Figure 10. A) Schematic illustration of the crystalline structure of 2D perovskites. B) Top view SEM images of the $(\text{IC}_2\text{H}_4\text{NH}_3)_2(\text{MA})_{n-1}\text{PbI}_{3n+1}$ perovskites prepared with different dipping durations. C) Cross-sectional SEM images of the $(\text{IC}_2\text{H}_4\text{NH}_3)_2(\text{MA})_{n-1}\text{PbI}_{3n+1}$ perovskites prepared with different dipping durations. D) Cross-sectional SEM images of the $(\text{IC}_2\text{H}_4\text{NH}_3)_2(\text{MA})_{n-1}\text{PbI}_{3n+1}$ perovskites based devices prepared with different dipping duration. E) J - V curves of standard 3D MAPbI₃ device without encapsulation in 25 °C 70%–80% relative humidity. F) Photovoltaic parameters of perovskite solar cells without encapsulation in 25 °C 70%–80% relative humidity fabricated with different dipping durations, after 1 day to 4 days.^[122]

influence of adding FEAI to a MAPbI₃ precursor solution on the resulting stability against moisture, two unencapsulated perovskite solar cells based on a reference perovskite the one with 3% FEAI were investigated. The perovskite with 3% FEAI still exhibited 92% of the initial PCE after storage for

120 days in air while the PCE of the device with pristine MAPbI₃ dropped 21% compared to its initial value (Figure 12B,C). Moreover, the powder XRD patterns of the samples were periodically recorded, as shown in Figure 12D,E, where the 3% FEAI-modified perovskite film



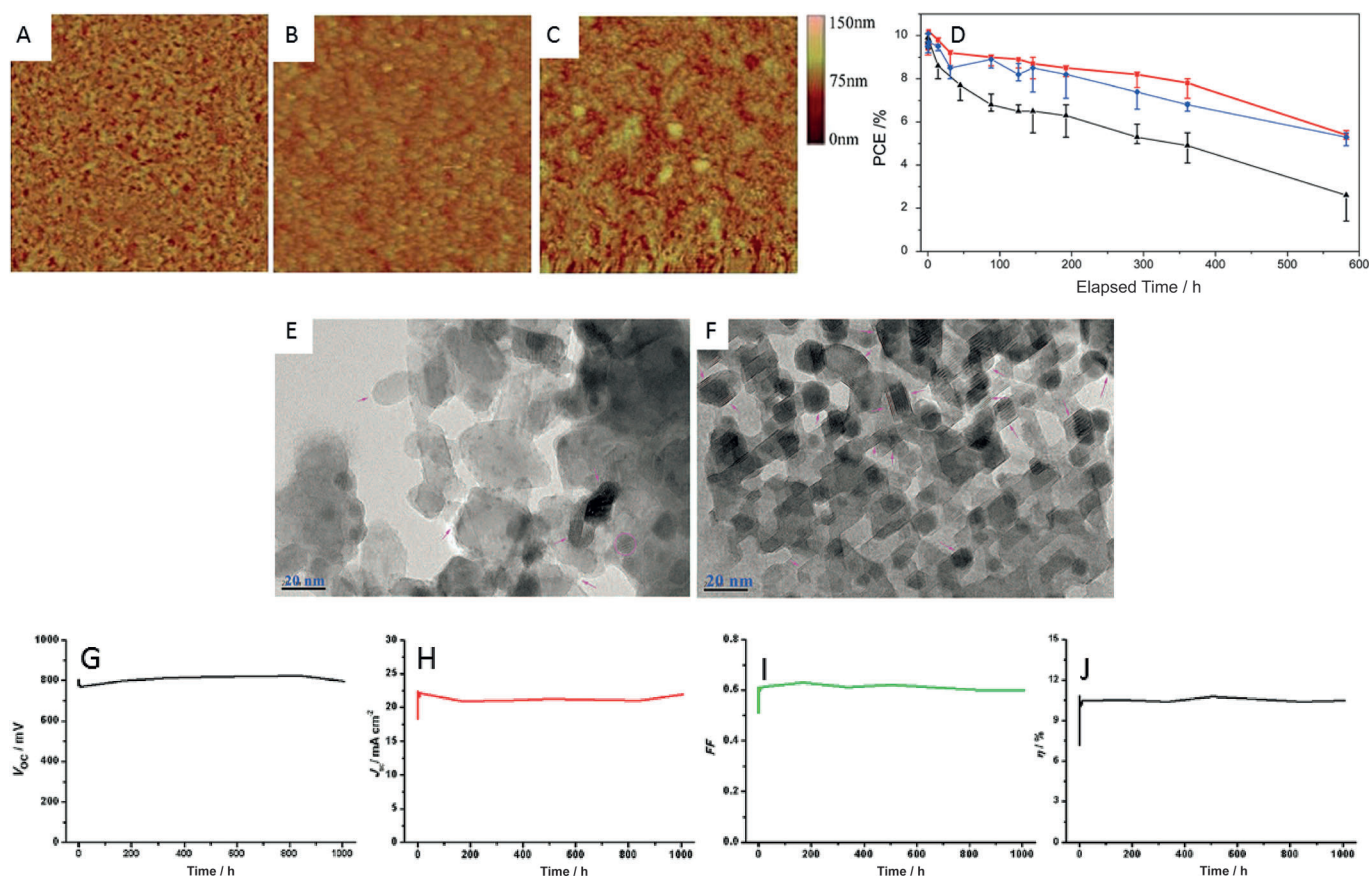


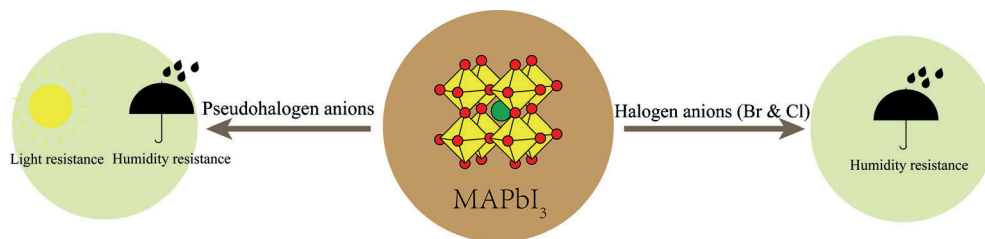
Figure 11. AFM topographical images of MAPbI_{3-x}Cl_x films prepared using A) 0%, B) 0.5%, and C) 1% concentrations of EAI. D) Long-term performances of perovskite solar cells, prepared using EAI at concentrations of 0% (black), 0.5% (blue), and 1% (red), at 65 °C after storage in the dark under Ar.^[128] TEM images of E) MAPbI₃ and F) (5-AVA)_x(MA)_(1-x)PbI₃ with TiO₂ mesoporous film that is infiltrated with perovskites. Stability of J) V_{oc}, H) J_{sc}, I) FF, and J) PCE for triple layer (5-AVA)_x(MA)_(1-x)PbI₃ perovskite solar cells in ambient air over 1008 h with an unsealed device.^[74]

exhibited much slower degradation to the new phase of PbI₂ after 40 days compared to the MAPbI₃ perovskite film. The improved stability may be attributed to the array of FEA cations stands on the surface of perovskite grains with their hydrophobic side facing outwards, protecting the perovskite crystal from direct interaction with water molecules (Figure 12F). Thus using hydrophobic fluorocarbons is an effective way to improve the micromorphology of the perovskite layer and give moisture-resistant properties to perovskite solar cells.

3. The Effect of Substitution of the X Anion on Stability

The anions, in organic-inorganic perovskite materials, are halogens, pseudo halides, tetrafluoroborate, or mixtures of them. They occupy the six vertices of the octahedral BX₆ structure in perovskites. The tetragonal structure of the perovskite

can be changed to the cubic structure when X halogen anions, for example, I⁻, are replaced by other anions because of their different radius. These structural distortions may remarkably affect the band gap, crystal structure, and charge transport of the perovskite. Moreover, the chemical reaction between hole-transporting materials (e.g., spiro-OMeTAD⁺) and migrating I⁻, which progressively reduces the conductivity of hole-transporting materials and deteriorates solar-cell stability and performance, can be significantly avoided.^[132] It is also possible to significantly improve the stability of perovskites by tuning the perovskite phase or by establishing strong interactions with the Pb ions,^[7,26,133] as shown in Scheme 3.



Scheme 3. Effect of anions and their substitutions on the stability of perovskite materials.

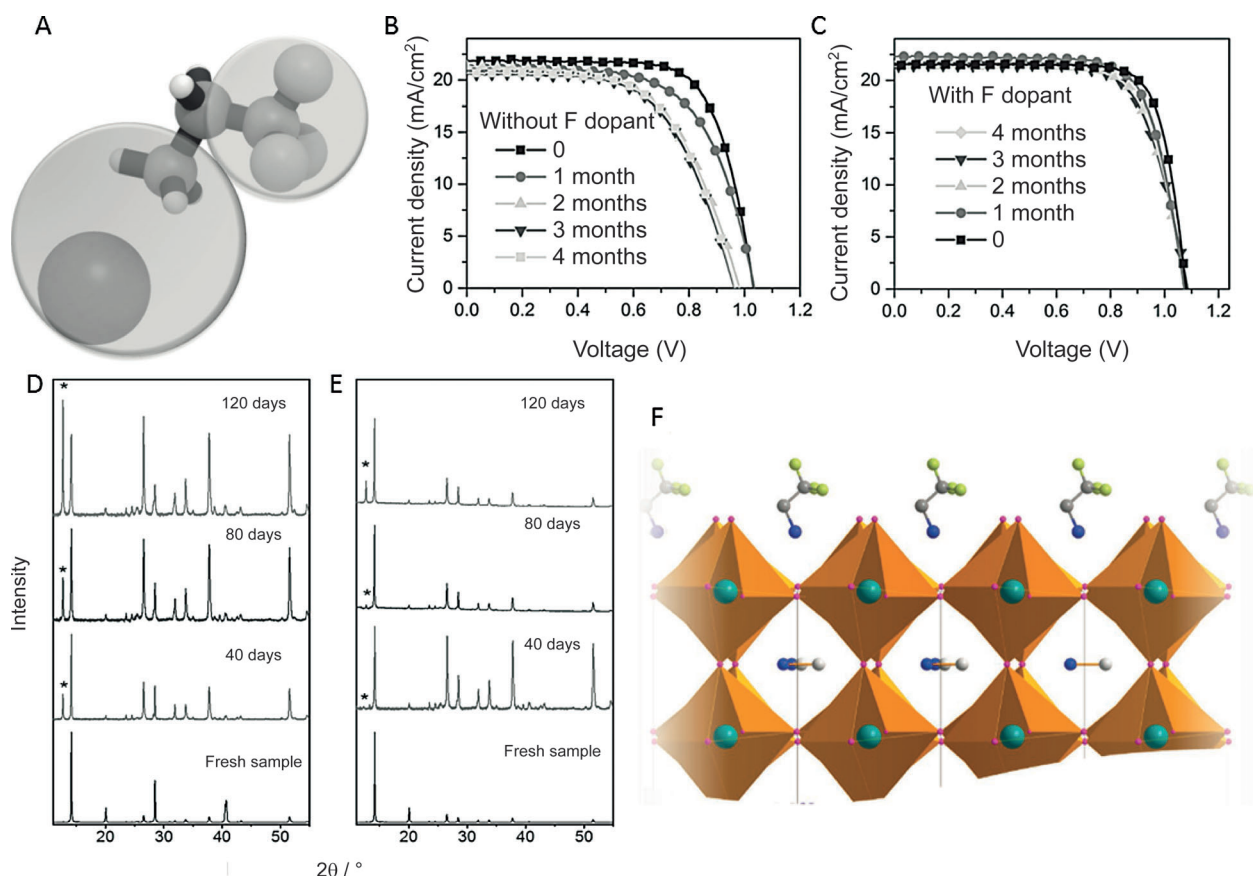


Figure 12. A) Structure of 1,1,1-trifluoroethyl ammonium iodide (FEAI). Aging test of the perovskite solar cell based MAPbI₃ (B), and with 3% FEAI (C), based on *J-V* curves under simulated AM 1.5G solar illumination. Powder XRD patterns of perovskite D) MAPbI₃ and E) MAPbI₃ + 3% FEAI under relative humidity of 30%. F) Diagram of the dispersion of FEAI in the MAPbI₃ structure.^[131]

3.1. Substitution of Halogen Anions

As homologues to iodine, chlorine and bromine have similar properties and suitable atomic radius for incorporation into perovskites. Sargent et al. successfully fabricated MAPbBr₃ and MAPbCl₃ perovskites which had increased band gaps but greatly improved stability.^[134] As shown in Figure 13, a new diffraction peak of PbI₂ appeared in the trace for MAPbI₃ after 7 days, indicating MAPbI₃ decomposed into PbI₂ while the MAPbBr₃ crystal was only slightly decomposed and the diffraction peak of MAPbCl₃ remained unchanged,

which suggests that chlorine and bromine could potentially improve the stability of perovskite as the cubic phase of MAPbBr₃ and MAPbCl₃ are much more stable.

Although the MAPbBr₃ and MAPbCl₃ perovskites showed enhanced stability, the device performance was greatly limited by their large band gaps. Mixed-halide perovskite, in which the iodide anion was partially substituted by bromide or chloride anions or by both of them, could significantly improve the stability of perovskite by controlling the composition without sacrificing cell performance. Mathews et al. could show that the addition of chloride by

a sequential deposition method enhanced the photovoltaic performance.^[135] In fact, incorporation of a small amount of Cl into MAPbI₃ could transform the crystal phase from tetragonal to a more stable cubic phase of MAPbI_{3-x}Cl_x at room temperature.^[136] Wu et al. fabricated a perovskite solar cell based on MAPbI_{3-x}Cl_x, which exhibiting long-term stability under humid conditions.^[137] More-

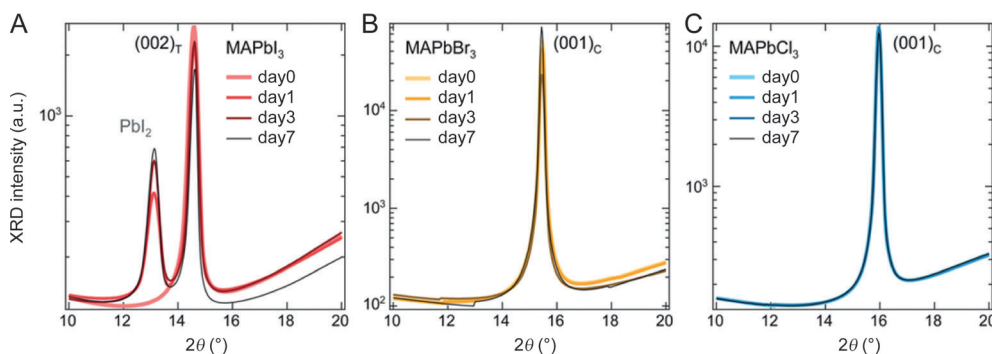


Figure 13. XRD curves of 2θ between 10 to 20 degrees for perovskite A) MAPbI₃, B) MAPbBr₃, C) MAPbCl₃ over 7 days.^[134]



over, retractable and flexibility solar cells based on $\text{MAPbI}_{3-x}\text{Cl}_x$ can even work stably for more than 96 h in humid conditions and fold more than 1000 times.^[138] Very recently, Dai et al. demonstrated for the first time a layer-by-layer growth of $\text{MAPbI}_{3-x}\text{Cl}_x$ perovskite, which is a solution-processed approach involving thermal evaporation of PbCl_2 , allowing for precise control over the thickness and to prepare uniform and compact perovskite films.^[139,140] Briefly, a thin layer of PbCl_2 (50 nm) is first deposited by thermal evaporation (Figure 14A). Subsequent dipping of the PbCl_2 into a solution of MAI in 2-propanol (10 mg mL^{-1}) transferred it into a layer of $\text{MAPbI}_{3-x}\text{Cl}_x$ perovskite. Similarly, a second PbCl_2 layer (50 nm) was thermally evaporated onto the newly formed $\text{MAPbI}_{3-x}\text{Cl}_x$ perovskite film, followed by dipping

into the MAI solution to form the second layer of $\text{MAPbI}_{3-x}\text{Cl}_x$ perovskite in close contacted with the underlying pre-formed $\text{MAPbI}_{3-x}\text{Cl}_x$ perovskite layer, and the process can be repeated (Steps 1 and 2, Figure 14A) several times to form an interface-free uniform $\text{MAPbI}_{3-x}\text{Cl}_x$ perovskite layer of the desired total thickness. A relatively good control of the content of Cl (6–8%) was achieved in every single layer, which is much higher than corresponding solution processed film. The reduced leak current and more compact morphology for the “multilayer” $\text{MAPbI}_{3-x}\text{Cl}_x$ perovskite film with respect to its solution-processed counterpart, explained the observed stability improvement. Accordingly, the perovskite solar cell based on layer-by-layer $\text{MAPbI}_{3-x}\text{Cl}_x$ retained 95 % of its initial PCE after storage in an Ar-filled glovebox

without any device encapsulation for 30 days while the PCE of the one-step solution-processed device dropped to 65 % of its original value under the same conditions (Figure 14B). The much better long-term stability observed for the layer-by-layer $\text{MAPbI}_{3-x}\text{Cl}_x$ perovskite solar cell can be attributed to the more compact and highly crystalline “multilayered” $\text{MAPbI}_{3-x}\text{Cl}_x$ perovskite pin-hole free film. Moreover, the pristine $\text{MAPbI}_{3-x}\text{Cl}_x$ perovskite film formed by the layer-by-layer approach exhibited slow degradation just at the film edge whereas the one-step solution-processed $\text{MAPbI}_{3-x}\text{Cl}_x$ perovskite film degraded completely into PbI_2 across the whole film after 21-day exposure to the ambient atmosphere (Figure 14C).

Seok and co-workers carried out the first partial substitution of I^- by Br^- to form $\text{MAPbI}_{3-x}\text{Br}_x$ perovskite, and realized a low-cost, highly efficient, long-term stable, and colored solar cells.^[26] The lattice parameter of $\text{MAPbI}_{3-x}\text{Br}_x$ phases exhibits a linear relationship with the Br content and the tetragonal to cubic phase transition point is between $x = 0.13$ and 0.20. In addition, with increasing of the value of x , the band gap of the perovskite gradually increases, which corresponds to the reduced lattice parameters. Band-gap tuning of mixed anion perovskites $\text{MAPb}(\text{I}_{1-x}\text{Br}_x)_2$ was also demon-

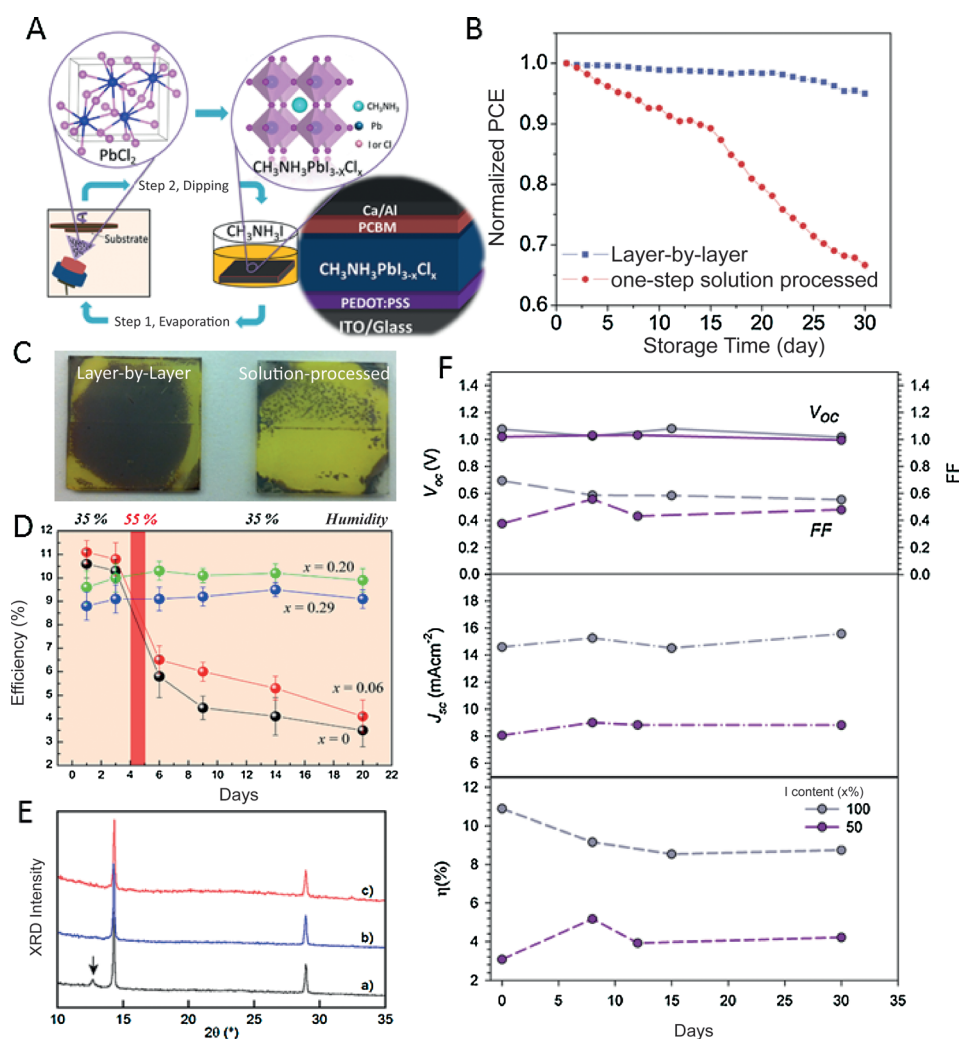


Figure 14. A) Device fabrication by layer-by-layer deposition. The procedure and the resulting device structure. B) PCE decay of the $\text{MAPbI}_{3-x}\text{Cl}_x$ perovskite solar cells fabricated by the layer-by-layer approach and one-step solution-processed method. C) Degradation of the $\text{MAPbI}_{3-x}\text{Cl}_x$ perovskite fabricated by the layer-by-layer approach and one-step solution-processed method after exposure to ambient atmosphere for 21 days.^[140] D) Stability of efficiency of $\text{MAPb}(\text{I}_{1-x}\text{Br}_x)_3$ ($x = 0, 0.06, 0.20, 0.29$) solar cells without encapsulation exposed to humidity of 35% for 20 days and 55% for a day.^[26] E) XRD of MAPbI_2Br thin films with MABr and PbI_2 solution in a ratio of 1:1 a) made in air, b) made in a glove box, and c) a ratio of 1.2:1 and made in air.^[41] F) Stability of V_{oc} , J_{sc} , FF, and PCE of $\text{MAPb}(\text{I}_{1-x}\text{Br}_x)_{3-y}\text{Cl}_y$ ($x = 0$ or 0.5) solar cells under 1 sun illumination. The devices have been stored in a glovebox under nitrogen atmosphere in the dark before being prepared for the individual measurements.^[43]

strated by Mathews et al. by means of a sequential deposition process.^[141] To investigate the stability of MAPbI_{3-x}Br_x ($x = 0, 0.06, 0.20, 0.29$) solar cells were exposed to moist air with a humidity of 35 % for 20 days, and the relative humidity was 55 % on the fifth day. As shown in Figure 14D, the efficiency slightly decreased in a humidity of 35 % and drastically decreased in humidity of 55 % for 20 days with $x = 0$ and 0.06 suggesting that MAPbI₃ and MAPbI_{3-x}Br_x with tetragonal phase are not stable in humidity; however, a stable efficiency has been maintained with $x = 0.20$ and 0.29, which may attribute to the stable cubic phase.

The MAPbI_{3-x}Br_x perovskite has also been investigated by Mosca et al.^[142] The crystal structure of MAPbI_{3-x}Br_x depends on the ratios of I and Br. When the value of x is less than 0.57, the perovskite structure is tetragonal, otherwise it is cubic. The best suitable ratio of MAI and PbBr₂ is 3:1, which provided a perovskite with the formula MAPbI₂Br, and the best PCE is 13.1 %. More important, this perovskite stability is also enhanced. In Figure 14E, three XRD curves of MAPbI₂Br thin films with MABr and PbI₂ precursor solution in a ratio of 1:1 a) made in air, b) made in glove box, and c) a ratio of 1.2:1 made in air. It is clearly seen that with the same 1:1 ratio of MABr and PbI₂ but with different fabrication conditions significantly influences the perovskite stability. The XRD curve has a clear PbI₂ diffraction peak in curve a in Figure 14E, while it does not appear in curve b in Figure 14E, indicating that MAPbI₂Br is not stable in air and easily decomposes into PbI₂. When MAPbI₂Br is made in air with a slight excess of MABr, however, no PbI₂ diffraction peak appears. With excess of Br⁻, the perovskite seems even more stable in air (Figure 14E).

Partly replacing I⁻ with Br⁻ in MAPbI₃ perovskites can significantly improve the perovskite stability. The stability of

ternary halogen perovskite MAPb(I_{1-x}Br_x)_{3-y}Cl_y has also been noticeably influenced by changing the ratio between I⁻ and Br⁻.^[26] Figure 14F shows the changes of V_{oc} , J_{sc} , FF, and PCE in 30 days with $x = 1$ or 0.5. To evaluate the stability of the photovoltaic parameters of MAPb(I_{1-x}Br_x)_{3-y}Cl_y solar cells with different Br content, the devices were stored in a glovebox under nitrogen atmosphere in the dark. The MAPbI_{3-y}Cl_y perovskite solar cell without Br, undergoes a PCE drop of 20 % in 30 days, however with 50 % Br content there is a notable increase of PCE of about 37 %.^[143] This increased may be caused by the rearrangement of 3D perovskite structure over time.

3.2. Substitution of Pseudohalogen Anions

Pseudohalogen anions with similar chemical characteristics and ion radius to real halogen anions can also influence the t value of perovskite structures.^[144] The thiocyanate anion (SCN⁻) is a stable pseudohalogen anion that has similar properties to I⁻, as has been demonstrated by the incorporation of SCN⁻ ions into the dye structure in dye-sensitized solar cells which can significantly enhance the charge transport and optical absorption.^[145] Liang et al. fabricated MAPbI_{3-x}(SCN)_x perovskite by a two-step solution method, in which a small amount of Pb(SCN)₂ was added to a PbI₂ solution.^[146] Large grains and fewer charge traps were achieved in the MAPbI_{3-x}(SCN)_x perovskite (Figure 15A,B), which is beneficial to device performance giving a best PCE of 11.07 %. Most importantly, the partial substitution of I⁻ by SCN⁻ in the perovskite structure can remarkably improve the stability compared to the traditional iodide-based perovskite. The PCE of the MAPbI_{3-x}(SCN)_x perovskite only dropped by

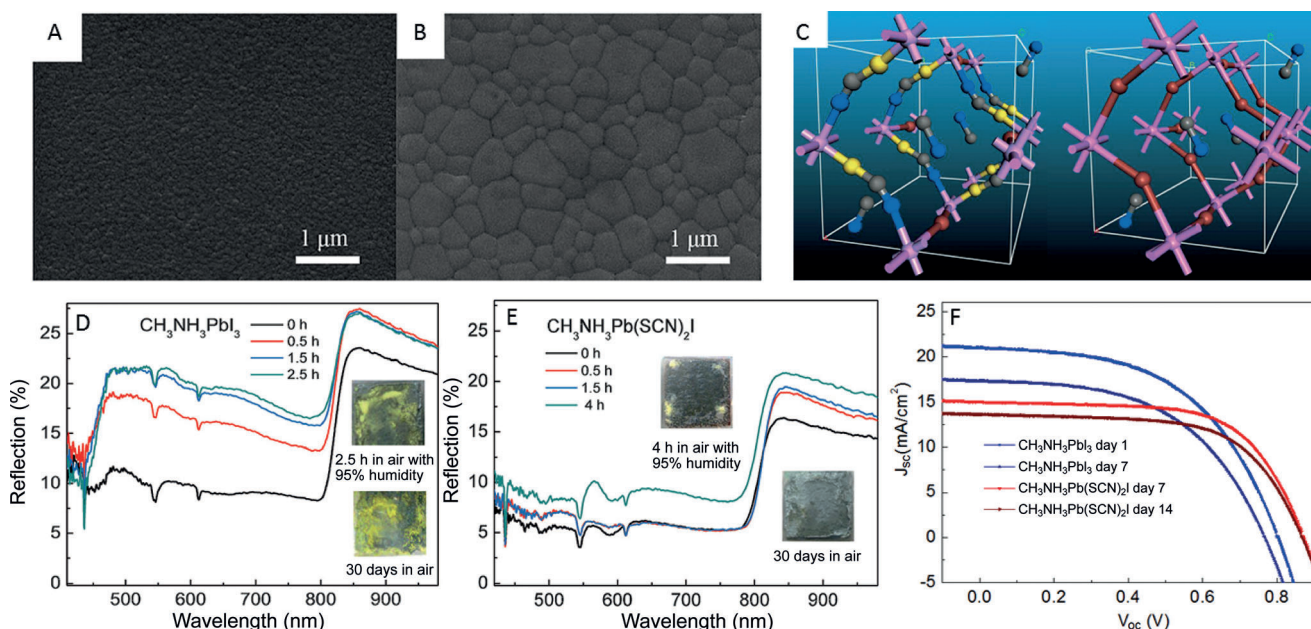


Figure 15. SEM images of A) MAPbI₃ and B) MAPbI_{3-x}(SCN)_x.^[146] C) Unit cell structure of MAPbI₃ (left) and MAPb(SCN)₂I (right) perovskites. Evolution of reflection curves of D) MAPbI₃ for 2.5 h and E) MAPb(SCN)₂I for 4 h in 95 % relative humidity air. F) J-V curves for MAPbI₃ and MAPb(SCN)₂I solar cells exposed to a relative humidity of 95 %.^[147]

8% while the MAPbI₃ perovskite dropped by 42% under 1 sun light irradiation for 1 h, indicating that light-induced degradation can dramatically be decreased by the incorporation of a little SCN[−] into the MAPbI₃ perovskite.

Xu et al. fabricated the MAPb(SCN)₂I perovskite by substituting I[−] in MAPbI₃ with two SCN[−] (Figure 15C).^[147] The formation constant was calculated to be 3.5 for PbI₄^{2−} in MAPbI₃ but 7 for Pb(SCN)₄^{2−} in MAPb(SCN)₂I,^[148,149] suggesting a more stable structure for MAPb(SCN)₂I since the formation constant of the lead halide complex reflects the binding tightness between the halides and the central Pb²⁺. Moreover, they recognized that linear shape of SCN[−] ions with lone pair electrons around the S and N atoms may strongly interact with the Pb²⁺ enhancing the electrostatic force more than is possible with the spherical I[−].^[147] The stability of MAPbI₃ and MAPb(SCN)₂I thin films exposed to 95% relative humidity air for several hours was first investigated in the reflection spectrum. A drastically increased reflection value for MAPbI₃ in 0.5 h indicates MAPbI₃ perovskite quickly degraded under humidity (Figure 15D). In contrast, the MAPb(SCN)₂I reflection value increased just a little under the same humidity for 4 h (Figure 15E). Moreover, the color of the MAPbI₃ film was almost completely changed to yellow in air for 30 days, indicating the formation of PbI₂, whereas no significant change was observed for MAPb(SCN)₂I. Finally, two perovskite solar cells based on MAPbI₃ and MAPb(SCN)₂I exposed to 95% relative humidity air were prepared, in which a PCE value of MAPbI₃ based device decreased from 8.8% to 6.9% in 7 days while that of the MAPb(SCN)₂I based device just decreased from 8.3% to 7.4% in 14 days. It is worth noting that the MAPbI₃ solar cell completely decomposed in 14 days.

In most cases, perovskite films have to be processed in an inert atmosphere, which hampers the commercial production and applications of the perovskite solar cells. Very recently, Yan et al. prepared high-quality MAPbI_{3−x}(SCN)_x in humidity air. The perovskite films and the related devices even when the relative humidity exceeds 70% in gave an average PCE of 13.49% and a maximum PCE over 15% (Figure 16A).^[150] In comparison with typical MAPbI₃-based devices which lose nearly 40% of the initial average PCE, the MAPbI_{3−x}(SCN)_x solar cells without encapsulation maintain 86.7% of their initial average PCE after being stored in air with the average humidity above 70% for over 500 h (Figure 16B). Calculations showed that the incorporation of SCN[−] groups into the perovskite lattice is thermodynamically stable (Figure 16C). Moreover, there are strong ionic interactions between SCN[−] and the adjacent Pb²⁺ ions and hydrogen bonds can form between SCN[−] and MA⁺, which should contribute to improved chemical stability. Clearly substitution of I[−] by SCN[−] in 3D MAPbI₃ enhances stability.

2D perovskite materials are more promising owing to their great improved stability as mentioned above. Scanlon et al. further investigated the 2D perovskite (MA)₂Pb(SCN)₂I₂, which exhibited a much greater improvement in stability.^[151] To explain the stability of this perovskite, they calculated the decomposition enthalpy and estimated its stability. MAPbI₃ readily decomposed into MAI and PbI₂ with a reaction enthalpy of −0.09 eV,^[152] however, (MA)₂Pb(SCN)₂I₂ can decompose in two ways: one is decomposition into MAI and Pb(SCN)₂ with a reaction enthalpy of 0.38 eV and the other is decomposition into MASCN and PbI₂ with a reaction enthalpy of 1.97 eV. Clearly the decomposition of (MA)₂Pb(SCN)₂I₂ is more difficult

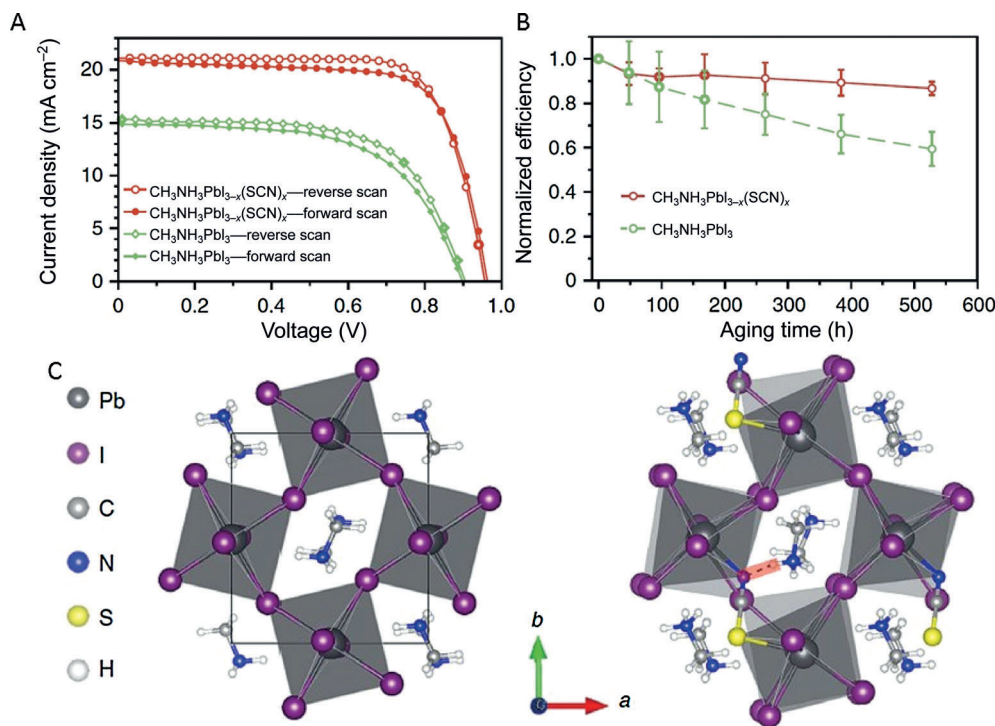
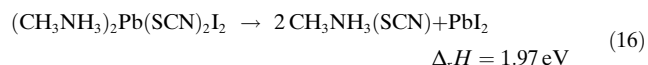
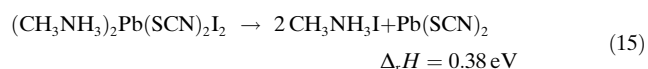
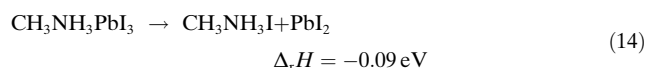


Figure 16. A) *J*–*V* curves of MAPbI_{3−x}(SCN)_x and MAPbI₃ solar cells prepared in ambient air. B) Evolution of the PCEs of MAPbI_{3−x}(SCN)_x and MAPbI₃ solar cells upon ageing in air without encapsulation. C) crystal structures of MAPbI₃ (left) and MAPbI_{3−x}(SCN)_x (right).^[150]

compared to MAPbI₃. Moreover, (MA)₂Pb(SCN)₂I₂ shows a suitable band gap, which may make it a promising material for perovskite solar cells applications [Eq. (14)–(16)].



4. Conclusions and Outlook

Herein, we have reviewed the recent advances in the substitution of A-cations/X-anions and their effect on the long-term stability of perovskites with regard to moisture, heat, light, and oxygen (see Table 1 and Table 2). The structural stability over thousands of hours under various conditions must be demonstrated, or else, the devices will probably not be attractive for commercial applications. Having elucidated the mechanisms of instability, we conclude that chemical modification has provided promising results with significantly enhanced stability. Partial substitution of FA⁺ by MA⁺ can give the α phase under low temperature and is beneficial to perovskite stability. Moreover, stability against moisture and light illumination can be remarkably enhanced by partly substituting FA⁺ by Cs⁺; the stability could be further improved with a mixture of three cations, Cs⁺/MA⁺/FA⁺. The preparation of 2D perovskite by the insertion of larger cations, for example, EA⁺, PEA⁺, FEA⁺, and 5-AVA⁺, into the 3D MAPbI₃ lattice can also improve stability compared to that of the 3D MAPbI₃ analogues, making them more attractive for large-scale industrial implementation.

Similar to cation substitution, various anions are also important to perovskite stability. The perovskite could be made more stable when anions (X) are Cl[−] or Br[−] are added as a result of the cubic MAPbCl₃ and MAPbBr₃ structure. In mixed anions perovskite, the presence of Br[−] is key to enhance perovskite stability in humidity or under illumination

Table 2: Effect of anions on stability.

Perovskite	Stability	Reference
MAPbBr ₃	Stable in cubic structure for 7 days	[133]
MAPbCl ₃	Stable in cubic structure for 7 days	[133]
MAPbI _{3-x} Br _x	Stable in air with a humidity of 35 % for 20 days	[26, 139, 140]
MAPbI _{3-x} Cl _x	Long term stability under humid conditions	[134–138]
MAPbI _{3-x} (SCN) _x	Improved stability under sunlight	[143, 147]
MAPb(SCN) ₂ I	Stable under a humidity of 95 % for 14 days	[144]
(MA) ₂ Pb(SCN) ₂ I ₂	Harder to decompose than MAPbI ₃	[148]

with only a slight sacrifice in device performance. Surprisingly, significantly enhanced moisture stability can be achieved through partly substituting I[−] by the pseudohalogen ion SCN[−] which also gives improved device performance. For perovskites with either A-cation or X-anion substitutions, the exposure to atmosphere is undesirable, and thus the development of effective encapsulation techniques is paramount. Moreover, understanding the photophysics and photochemistry processes, unraveling interfacial carrier accumulation as well as exploring effective methods to promote the growth of mixed cation and anion perovskite crystal are still need to be addressed.

Perovskites are particularly attractive for photovoltaic applications because they can be processed in solution, from cheap earth-abundant materials, and give high device performance that is competitive with established commercial technologies. The most frequent question is their long-term operational stability. Understanding the multifaceted chemistry of perovskites will be key for developing new materials that will bring this nascent technology to fruition. Manipulating this extraordinarily versatile platform through chemical modification could be a promising way for improving stability. There are still very few species that have been used as A-cations and X-anions. The substitution of new cations and anions, such as alkali-metal cations: Li⁺, Na⁺, K⁺, and Rb⁺, transition-metal cations: such as, Cu⁺, Ag⁺, and Au⁺, pseudohalide anions: CN[−], OCN[−], and SeCN[−], will be an essential part of future perovskite materials. Moreover,

Table 1: Effect of cations on stability.

Perovskite	Stability	Reference
FAPbI ₃	Thermally stable at 230 °C and light stable in humid conditions	[94–96, 98, 101, 103]
FA _{1-x} MA _x PbI ₃	Stable in humid conditions	[102, 104]
FASnI ₃	Stored in a humidity of 25 % for more than 100 days	[97]
CsPbI ₃ Br _(3-x)	Stable under humidity, heat, and light	[108–111]
CsPbI ₃	Thermally stable	[107]
Cs _x (MA _{0.17} FA _{0.83}) _(100-x) Pb(I _{0.83} Br _{0.17}) ₃	Stable at 130 °C in dry air for 3 h and stable under constant illumination for 250 h	[114]
FA _{0.85} Cs _{0.15} PbI ₃	Stable under light and humid conditions	[112]
(PEA) ₂ (MA) ₂ [Pb ₃ I ₁₀]	Stable under a humidity of 50 %	[117]
PEA ₂ (MA) _{n-1} Pb _{n-1} I _{3n+1}	Stable for 60 days in a humid atmosphere	[118]
(CH ₃ (CH ₂) ₃ NH ₃) ₂ (MA) _{n-1} Pb _{n-1} I _{3n+1}	Stable in a humid atmosphere for two months	[119]
(IC ₂ H ₄ NH ₃) ₂ (MA) _{n-1} Pb _{n-1} I _{3n+1}	Stable in relative humidity of 70–80 %	[121]
(MAPbI ₃) _{1-x} [(PEI) ₂ PbI ₄] _x	Stable in humidity of 50 % for 16 days	[123]
(5-AVA) _x (MA) _{1-x} PbI ₃	Stable more than 1000 h in humid air	[74]
FEA cations in MAPbI ₃	Stable under humid conditions for more than 120 days	[127]



multiple cation and anion mixtures (more than three) maybe another compositional strategy to improve both stability and performance for perovskite solar cells. In 2D perovskites, one way is to replace MA^+ by FA^+ to further reduce the band gap in 2D perovskites and another direction is to explore novel large organic cations, so that solar devices with even higher performance without hysteresis could potentially be engineered in the future. In addition, standards of measurements, for example, the International Electrotechnical Commission (IEC) 61646 “Thin-film terrestrial photovoltaic (PV) modules—Design qualification and type approval” or IEC 61215 “Crystalline silicon terrestrial photovoltaic (PV) modules—Design qualification and type approval”, have not yet been filed for perovskite solar cells and must be done in the next few years. Further challenges to be resolved include the unreliable device performance, for example, hysteresis, and the inherent toxicity of the lead in the structure. We have great confidence that, with further progress, the benefits of perovskites with their great compositional tunability can give researchers hope to solve the challenges and prepare robust solar cells.

Acknowledgments

This work was financially supported by the National Basic Research Program of China-Fundamental Studies of Perovskite Solar Cells (2015CB932200) and Startup from Nanjing Tech University (3983500160, ZKRC201514).

- [1] W. G. Pfann, W. Van Roosbroeck, *J. Appl. Phys.* **1954**, 25, 1422–1434.
- [2] J. Yan, B. R. Saunders, *RSC Adv.* **2014**, 4, 43286–43314.
- [3] W. S. Yang, J. H. Noh, N. J. Jeon, Y. C. Kim, S. Ryu, J. Seo, S. I. Seok, *Science* **2015**, 348, 1234–1237.
- [4] http://www.nrel.gov/ncpv/images/efficiency_chart.jpg **2016**.
- [5] a) M. M. Lee, J. Teuscher, T. Miyasaka, T. N. Murakami, H. J. Snaith, *Science* **2012**, 338, 643–647; b) J. S. Manser, M. I. Saidaminov, J. A. Christians, O. M. Bakr, P. V. Kamat, *Acc. Chem. Res.* **2016**, 49, 330–338; c) Z. Xiao, Y. Yuan, Q. Wang, Y. Shao, Y. Bai, Y. Deng, Q. Dong, M. Hu, C. Bi, J. Huang, *Mater. Sci. Eng. R* **2016**, 101, 1–38; d) M. Saba, F. Quochi, A. Mura, G. Bongiovanni, *Acc. Chem. Res.* **2016**, 49, 166–173; e) M. B. Johnston, L. M. Herz, *Acc. Chem. Res.* **2016**, 49, 146–154; f) L. Meng, J. You, T.-F. Guo, Y. Yang, *Acc. Chem. Res.* **2016**, 49, 155–165; g) C. Zuo, H. J. Bolink, H. Han, J. Huang, D. Cahen, L. Ding, *Adv. Sci.* **2016**, DOI: 10.1002/advs.201500324; h) S. D. Stranks, P. K. Nayak, W. Zhang, T. Stergiopoulos, H. J. Snaith, *Angew. Chem. Int. Ed.* **2015**, 54, 3240–3248; *Angew. Chem.* **2015**, 127, 3288–3297; i) C. C. Stoumpos, M. G. Kanatzidis, *Acc. Chem. Res.* **2015**, 48, 2791–2802; j) B. V. Lotsch, *Angew. Chem. Int. Ed.* **2014**, 53, 635–637; *Angew. Chem.* **2014**, 126, 647–649; k) T. C. Sum, M. Mathews, *Energy Environ. Sci.* **2014**, 7, 2518–2534; l) P. Gao, M. Grätzel, M. K. Nazeeruddin, *Energy Environ. Sci.* **2014**, 7, 2448–2463; m) S. Kazim, M. K. Nazeeruddin, M. Grätzel, S. Ahmad, *Angew. Chem. Int. Ed.* **2014**, 53, 2812–2824; *Angew. Chem.* **2014**, 126, 2854–2867.
- [6] M. A. Green, A. Ho-Baillie, H. J. Snaith, *Nat. Photonics* **2014**, 8, 506–514.
- [7] Z. Cheng, J. Lin, *CrystEngComm* **2010**, 12, 2646–2662.
- [8] A. Poglitsch, D. Weber, *J. Chem. Phys.* **1987**, 87, 6373–6378.
- [9] C. C. Stoumpos, C. D. Malliakas, M. G. Kanatzidis, *Inorg. Chem.* **2013**, 52, 9019–9038.
- [10] P. P. Boix, K. Nonomura, N. Mathews, S. G. Mhaisalkar, *Mater. Today* **2014**, 17, 16–23.
- [11] J. H. Heo, D. H. Song, B. R. Patil, S. H. Im, *Isr. J. Chem.* **2015**, 55, 966–977.
- [12] A. Kojima, K. Teshima, Y. Shirai, T. Miyasaka, *J. Am. Chem. Soc.* **2009**, 131, 6050–6051.
- [13] C. Wehrenfennig, G. E. Eperon, M. B. Johnston, H. J. Snaith, L. M. Herz, *Adv. Mater.* **2014**, 26, 1584–1589.
- [14] V. D’Innocenzo, G. Grancini, M. J. P. Alcocer, A. R. S. Kandada, S. D. Stranks, M. M. Lee, G. Lanzani, H. J. Snaith, A. Petrozza, *Nat. Commun.* **2014**, 5, 3586.
- [15] G. Xing, N. Mathews, S. Sun, S. S. Lim, Y. M. Lam, M. Graetzel, S. Mhaisalkar, T. C. Sum, *Science* **2013**, 342, 344–347.
- [16] S. D. Stranks, G. E. Eperon, G. Grancini, C. Menelaou, M. J. P. Alcocer, T. Leijtens, L. M. Herz, A. Petrozza, H. J. Snaith, *Science* **2013**, 342, 341–344.
- [17] S. Chen, K. R. Choudhury, J. Subbiah, C. M. Amb, J. R. Reynolds, F. So, *Adv. Energy Mater.* **2011**, 1, 963–969.
- [18] P. Docampo, T. Bein, *Acc. Chem. Res.* **2016**, 49, 339–346.
- [19] Y. Rong, L. Liu, A. Mei, X. Li, H. Han, *Adv. Energy Mater.* **2015**, 5, 1501066.
- [20] T. Leijtens, G. E. Eperon, N. K. Noel, S. N. Habisreutinger, A. Petrozza, H. J. Snaith, *Adv. Energy Mater.* **2015**, 5, 1500963.
- [21] T. A. Berhe, W. Su, C. Chen, C. Pan, J. Cheng, H. Chen, M. Tsai, L. Chen, A. A. Dubale, B. Hwang, *Energy Environ. Sci.* **2016**, 9, 323–356.
- [22] M. Ye, X. Hong, F. Zhang, X. Liu, *J. Mater. Chem. A* **2016**, 4, 6755–6771.
- [23] H. T. Nguyen, Z. Ku, H. J. Fan, *Adv. Energy Mater.* **2016**, 6, 1501420.
- [24] A. B. Djurisic, F. Liu, A. M. C. Ng, Q. Dong, M. K. Wong, A. Ng, C. Surya, *Phys. Status Solidi RRL* **2016**, 10, 281–299.
- [25] B. Li, Y. Li, C. Zheng, D. Gao, W. Huang, *RSC Adv.* **2016**, 6, 38079–38091.
- [26] J. H. Noh, S. H. Im, J. H. Heo, T. N. Mandal, S. I. Seok, *Nano Lett.* **2013**, 13, 1764–1769.
- [27] G. Niu, W. Li, F. Meng, L. Wang, H. Dong, Y. Qiu, *J. Mater. Chem. A* **2014**, 2, 705–710.
- [28] C. Clegg, I. G. Hill, *RSC Adv.* **2016**, 6, 5244852458.
- [29] S. Ahmad, P. K. Kanaujia, W. Niu, J. J. Baumberg, G. V. Prakash, *ACS Appl. Mater. Interfaces* **2014**, 6, 10238–10247.
- [30] J. M. Frost, K. T. Butler, F. Brivio, C. H. Hendon, M. van Schilfegaarde, A. Walsh, *Nano Lett.* **2014**, 14, 2584–2590.
- [31] B. Conings, J. Drijkoningen, N. Gauquelin, A. Babayigit, J. D’Haen, L. D’Olieslaeger, A. Ethirajan, J. Verbeeck, J. Manca, E. Mosconi, F. De Angelis, H. Boyen, *Adv. Energy Mater.* **2015**, 5, 1500477.
- [32] Y. Dkhissi, S. Meyer, D. Chen, H. C. Weerasinghe, L. Spiccia, Y. Cheng, R. A. Caruso, *ChemSusChem* **2016**, 9, 687–695.
- [33] J. H. Heo, S. H. Im, J. H. Noh, T. N. Mandal, C. Lim, J. A. Chang, Y. H. Lee, H. Kim, A. Sarkar, M. K. Nazeeruddin, M. Graetzel, S. I. Seok, *Nat. Photonics* **2013**, 7, 486–491.
- [34] G. Divitini, S. Cacovich, F. Matteocci, L. Cinà, A. Di Carlo, C. Ducati, *Nat. Energy* **2016**, 1, 15012.
- [35] D. Bryant, N. Aristidou, S. Pont, I. Sanchez-Molina, T. Chotchunangatchaval, S. Wheeler, J. R. Durrant, S. A. Haque, *Energy Environ. Sci.* **2016**, 9, 1655–1660.
- [36] H. Yuan, E. Debroye, K. Janssen, H. Naiki, C. Steuwe, G. Lu, M. Moris, E. Orgiu, H. Uji-i, F. De Schryver, P. Samori, J. Hofkens, M. Roelofs, *J. Phys. Chem. Lett.* **2016**, 7, 561–566.
- [37] T. Leijtens, G. E. Eperon, S. Pathak, A. Abate, M. M. Lee, H. J. Snaith, *Nat. Commun.* **2013**, 4, 2885.
- [38] S. Ito, S. Tanaka, K. Manabe, H. Nishino, *J. Phys. Chem. C* **2014**, 118, 16995–17000.

- [39] D. Wei, T. Wang, J. Ji, M. Li, P. Cui, Y. Li, G. Li, J. M. Mbengue, D. Song, *J. Mater. Chem. A* **2016**, *4*, 1991–1998.
- [40] N. Aristidou, I. Sanchez-Molina, T. Chotchuanchuchaval, M. Brown, L. Martinez, T. Rath, S. A. Haque, *Angew. Chem. Int. Ed.* **2015**, *54*, 8208–8212; *Angew. Chem.* **2015**, *127*, 8326–8330.
- [41] A. J. Pearson, G. E. Eperon, P. E. Hopkinson, S. N. Habisreutinger, J. T. Wang, H. J. Snaith, N. C. Greenham, *Adv. Energy Mater.* **2016**, DOI: 10.1002/aenm.201600014.
- [42] W. Li, W. Zhang, S. Van Reenen, R. J. Sutton, J. Fan, A. A. Haghighirad, M. B. Johnston, L. Wang, H. J. Snaith, *Energy Environ. Sci.* **2016**, *9*, 490–498.
- [43] H. Si, Q. Liao, Z. Zhang, Y. Li, X. Yang, G. Zhang, Z. Kang, Y. Zhang, *Nano Energy* **2016**, *22*, 223–231.
- [44] X. Dong, X. Fang, M. Lv, B. Lin, S. Zhang, J. Ding, N. Yuan, *J. Mater. Chem. A* **2015**, *3*, 5360–5367.
- [45] S. Guarnera, A. Abate, W. Zhang, J. M. Foster, G. Richardson, A. Petrozza, H. J. Snaith, *J. Phys. Chem. Lett.* **2015**, *6*, 432–437.
- [46] W. Li, H. Dong, L. Wang, N. Li, X. Guo, J. Li, Y. Qiu, *J. Mater. Chem. A* **2014**, *2*, 13587–13592.
- [47] Q. Wang, Q. Dong, T. Li, A. Gruverman, J. Huang, *Adv. Mater.* **2016**, DOI: 10.1002/adma.201600969.
- [48] W. Li, J. Li, G. Niu, L. Wang, *J. Mater. Chem. A* **2016**, DOI: 10.1039/c5ta09165a.
- [49] Y. Hou, H. Zhang, W. Chen, S. Chen, C. O. R. Quiroz, H. Azimi, A. Osvet, G. J. Matt, E. Zeira, J. Seuring, N. Kausch-Busies, W. Loevenich, C. J. Brabec, *Adv. Energy Mater.* **2015**, *5*, 1500543.
- [50] A. Agresti, S. Pescetelli, L. Cina, D. Konios, G. Kakavelakis, E. Kymakis, A. Di Carlo, *Adv. Funct. Mater.* **2016**, *26*, 2686–2694.
- [51] W. Chen, Y. Wu, Y. Yue, J. Liu, W. Zhang, X. Yang, H. Chen, E. Bi, I. Ashraful, M. Graetzel, L. Han, *Science* **2015**, *350*, 944–948.
- [52] J. You, L. Meng, T. Song, T. Guo, Y. M. Yang, W. Chang, Z. Hong, H. Chen, H. Zhou, Q. Chen, Y. Liu, N. De Marco, Y. Yang, *Nat. Nanotechnol.* **2016**, *11*, 75–81.
- [53] S. N. Habisreutinger, T. Leijtens, G. E. Eperon, S. D. Stranks, R. J. Nicholas, H. J. Snaith, *Nano Lett.* **2014**, *14*, 5561–5568.
- [54] J. Liu, S. Pathak, T. Stergiopoulos, T. Leijtens, K. Wojciechowski, S. Schumann, N. Kausch-Busies, H. J. Snaith, *J. Phys. Chem. Lett.* **2015**, *6*, 1666–1673.
- [55] Y. S. Kwon, J. Lim, H. Yun, Y. Kim, T. Park, *Energy Environ. Sci.* **2014**, *7*, 1454–1460.
- [56] J. Liu, Y. Wu, C. Qin, X. Yang, T. Yasuda, A. Islam, K. Zhang, W. Peng, W. Chen, L. Han, *Energy Environ. Sci.* **2014**, *7*, 2963–2967.
- [57] L. Zheng, Y. Chung, Y. Ma, L. Zhang, L. Xiao, Z. Chen, S. Wang, B. Qu, Q. Gong, *Chem. Commun.* **2014**, *50*, 11196–11199.
- [58] H. Li, K. Fu, A. Hagfeldt, M. Graetzel, S. G. Mhaisalkar, A. C. Grimsdale, *Angew. Chem. Int. Ed.* **2014**, *53*, 4085–4088; *Angew. Chem.* **2014**, *126*, 4169–4172.
- [59] J. Xiao, J. Shi, H. Liu, Y. Xu, S. Lv, Y. Luo, D. Li, Q. Meng, Y. Li, *Adv. Energy Mater.* **2015**, *5*, 1401943.
- [60] H. Choi, S. Park, S. Paek, P. Ekanayake, M. K. Nazeeruddin, J. Ko, *J. Mater. Chem. A* **2014**, *2*, 19136–19140.
- [61] Y. Ma, Y. Chung, L. Zheng, D. Zhang, X. Yu, L. Xiao, Z. Chen, S. Wang, B. Qu, Q. Gong, D. Zou, *ACS Appl. Mater. Interfaces* **2015**, *7*, 6406–6411.
- [62] J. Min, Z. Zhang, Y. Hou, C. O. R. Quiroz, T. Przybilla, C. Bronnbauer, F. Guo, K. Forberich, H. Azimi, T. Ameri, E. Spiecker, Y. Li, C. J. Brabec, *Chem. Mater.* **2015**, *27*, 227–234.
- [63] K. Neumann, M. Thelakkat, *RSC Adv.* **2014**, *4*, 43550–43559.
- [64] H. Choi, J. W. Cho, M. Kang, J. Ko, *Chem. Commun.* **2015**, *51*, 9305–9308.
- [65] M. Zhang, M. Lyu, H. Yu, J. Yun, Q. Wang, L. Wang, *Chem. Eur. J.* **2015**, *21*, 434–439.
- [66] S. N. Habisreutinger, T. Leijtens, G. E. Eperon, S. D. Stranks, R. J. Nicholas, H. J. Snaith, *J. Phys. Chem. Lett.* **2014**, *5*, 4207–4212.
- [67] J. Zhang, Z. Hu, L. Huang, G. Yue, J. Liu, X. Lu, Z. Hu, M. Shang, L. Han, Y. Zhu, *Chem. Commun.* **2015**, *51*, 7047–7050.
- [68] J. Cao, J. Yin, S. Yuan, Y. Zhao, J. Li, N. Zheng, *Nanoscale* **2015**, *7*, 9443–9447.
- [69] Z. Zhu, C. Chueh, F. Lin, A. K. Y. Jen, *Adv. Sci.* **2016**, *3*, 1600027.
- [70] B. Roose, K. C. Gödel, S. Pathak, A. Sadhanala, J. P. C. Baena, B. D. Wilts, H. J. Snaith, U. Wiesner, M. Grätzel, U. Steiner, A. Abate, *Adv. Energy Mater.* **2015**, *5*, 1501868.
- [71] M. M. Tavakoli, R. Tavakoli, Z. Nourbakhsh, A. Waleed, U. S. Virk, Z. Fan, *Adv. Mater. Interfaces* **2016**, *3*, 1500790.
- [72] S. Yang, Y. Wang, P. Liu, Y. Cheng, H. J. Zhao, H. G. Yang, *Nat. Energy* **2016**, *1*, 15016.
- [73] F. Zhang, X. Yang, M. Cheng, W. Wang, L. Sun, *Nano Energy* **2016**, *20*, 108–116.
- [74] A. Mei, X. Li, L. Liu, Z. Ku, T. Liu, Y. Rong, M. Xu, M. Hu, J. Chen, Y. Yang, M. Graetzel, H. Han, *Science* **2014**, *345*, 295–298.
- [75] X. Li, M. Tschumi, H. Han, S. S. Babkair, R. A. Alzubaydi, A. A. Ansari, S. S. Habib, M. K. Nazeeruddin, S. M. Zakeeruddin, M. Graetzel, *Energy Technol.* **2015**, *3*, 551–555.
- [76] X. Xu, Z. Liu, Z. Zuo, M. Zhang, Z. Zhao, Y. Shen, H. Zhou, Q. Chen, Y. Yang, M. Wang, *Nano Lett.* **2015**, *15*, 2402–2408.
- [77] F. Zhang, X. Yang, H. Wang, M. Cheng, J. Zhao, L. Sun, *ACS Appl. Mater. Interfaces* **2014**, *6*, 16140–16146.
- [78] Y. Rong, Z. Ku, A. Mei, T. Liu, M. Xu, S. Ko, X. Li, H. Han, *J. Phys. Chem. Lett.* **2014**, *5*, 2160–2164.
- [79] H. Zhou, Y. Shi, K. Wang, Q. Dong, X. Bai, Y. Xing, Y. Du, T. Ma, *J. Phys. Chem. A* **2015**, *119*, 4600–4605.
- [80] K. M. Boopathi, R. Mohan, T. Huang, W. Budiawan, M. Lin, C. Lee, K. Ho, C. Chu, *J. Mater. Chem. A* **2016**, *4*, 1591–1597.
- [81] X. Li, M. I. Dar, C. Yi, J. Luo, M. Tschumi, S. M. Zakeeruddin, M. K. Nazeeruddin, H. Han, M. Graetzel, *Nat. Chem.* **2015**, *7*, 703–711.
- [82] A. Abate, M. Saliba, D. J. Hollman, S. D. Stranks, K. Wojciechowski, R. Avolio, G. Grancini, A. Petrozza, H. J. Snaith, *Nano Lett.* **2014**, *14*, 3247–3254.
- [83] B. Wang, T. Chen, *Adv. Sci.* **2016**, *3*, 1500262.
- [84] S. Casaluci, L. Cinà, A. Pockett, P. S. Kubiak, R. G. Niemann, A. Reale, A. Di Carlo, P. J. Cameron, *J. Power Sources* **2015**, *297*, 504–510.
- [85] D. Yang, Z. Yang, W. Qin, Y. Zhang, S. F. Liu, C. Li, *J. Mater. Chem. A* **2015**, *3*, 9401–9405.
- [86] L. Q. Zhang, X. W. Zhang, Z. G. Yin, Q. Jiang, X. Liu, J. H. Meng, Y. J. Zhao, H. L. Wang, *J. Mater. Chem. A* **2015**, *3*, 12133–12138.
- [87] J. J. Zhao, P. Wang, Z. H. Liu, L. Y. Wei, Z. Yang, H. R. Chen, X. Q. Fang, X. L. Liu, Y. H. Mai, *Dalton Trans.* **2015**, *44*, 17841–17849.
- [88] K. A. Bush, C. D. Bailie, Y. Chen, A. R. Bowring, W. Wang, W. Ma, T. Leijtens, F. Moghadam, M. D. McGehee, *Adv. Mater.* **2016**, *28*, 3937–3943.
- [89] C. Motta, F. El-Mellouhi, S. Kais, N. Tabet, F. Alharbi, S. Sanvito, *Nat. Commun.* **2015**, *6*, 7026.
- [90] Y. Zhao, K. Zhu, *Chem. Soc. Rev.* **2016**, *45*, 655–689.
- [91] T. M. Koh, K. Fu, Y. Fang, S. Chen, T. C. Sum, N. Mathews, S. G. Mhaisalkar, P. P. Boix, T. Baikie, *J. Phys. Chem. C* **2014**, *118*, 16458–16462.
- [92] A. Amat, E. Mosconi, E. Ronca, C. Quarti, P. Umari, M. K. Nazeeruddin, M. Graetzel, F. De Angelis, *Nano Lett.* **2014**, *14*, 3608–3616.
- [93] G. E. Eperon, S. D. Stranks, C. Menelaou, M. B. Johnston, L. M. Herz, H. J. Snaith, *Energy Environ. Sci.* **2014**, *7*, 982–988.
- [94] I. Borriello, G. Cantele, D. Ninno, *Phys. Rev. B* **2008**, *77*, 235214.



- [95] J. Lee, D. Seol, A. Cho, N. Park, *Adv. Mater.* **2014**, *26*, 4991–4998.
- [96] F. Wang, H. Yu, H. Xu, N. Zhao, *Adv. Funct. Mater.* **2015**, *25*, 1120–1126.
- [97] M. R. Leyden, M. V. Lee, S. R. Raga, Y. Qi, *J. Mater. Chem. A* **2015**, *3*, 16097–16103.
- [98] S. J. Lee, S. S. Shin, Y. C. Kim, D. Kim, K. A. Tae, J. H. Noh, J. Seo, S. I. Seok, *J. Am. Chem. Soc.* **2016**, *138*, 3974–3977.
- [99] Y. Fu, H. Zhu, A. W. Schrader, D. Liang, Q. Ding, P. Joshi, L. Hwang, X. Zhu, S. Jin, *Nano Lett.* **2016**, *16*, 1000–1008.
- [100] A. Binek, F. C. Hanusch, P. Docampo, T. Bein, *J. Phys. Chem. Lett.* **2015**, *6*, 1249–1253.
- [101] F. Wang, J. Ma, F. Xie, L. Li, J. Chen, J. Fan, N. Zhao, *Adv. Funct. Mater.* **2016**, *26*, 3417–3423.
- [102] J. Lee, D. Kim, H. Kim, S. Seo, S. M. Cho, N. Park, *Adv. Energy Mater.* **2015**, *5*, 1501310.
- [103] D. B. Mitzi, K. Liang, *J. Solid State Chem.* **1997**, *134*, 376–384.
- [104] G. Murugadoss, S. Tanaka, G. Mizuta, S. Kanaya, H. Nishino, T. Umeyama, H. Imahori, S. Ito, *Jpn. J. Appl. Phys.* **2015**, *54*, 08KF08.
- [105] S. Aharon, A. Dymshits, A. Rotem, L. Etgar, *J. Mater. Chem. A* **2015**, *3*, 9171–9178.
- [106] N. J. Jeon, J. H. Noh, W. S. Yang, Y. C. Kim, S. Ryu, J. Seo, S. I. Seok, *Nature* **2015**, *517*, 476–480.
- [107] N. Pellet, P. Gao, G. Gregori, T. Yang, M. K. Nazeeruddin, J. Maier, M. Grätzel, *Angew. Chem. Int. Ed.* **2014**, *53*, 3151–3157; *Angew. Chem.* **2014**, *126*, 3215–3221.
- [108] G. E. Eperon, G. M. Paternò, R. J. Sutton, A. Zampetti, A. A. Haghighirad, F. Cacialli, H. J. Snaith, *J. Mater. Chem. A* **2015**, *3*, 19688–19695.
- [109] R. J. Sutton, G. E. Eperon, L. Miranda, E. S. Parrott, B. A. Kamino, J. B. Patel, M. T. Hörantner, M. B. Johnston, A. A. Haghighirad, D. T. Moore, H. J. Snaith, *Adv. Energy Mater.* **2016**, *6*, 1502458.
- [110] Q. Ma, S. Huang, X. Wen, M. A. Green, A. W. Y. Ho-Baillie, *Adv. Energy Mater.* **2016**, *6*, 1502202.
- [111] R. E. Beal, D. J. Slotcavage, T. Leijtens, A. R. Bowring, R. A. Belisle, W. H. Nguyen, G. F. Burkhard, E. T. Hoke, M. D. McGehee, *J. Phys. Chem. Lett.* **2016**, *7*, 746–751.
- [112] M. Kulbak, S. Gupta, N. Kedem, I. Levine, T. Bendikov, G. Hodes, D. Cahen, *J. Phys. Chem. Lett.* **2016**, *7*, 167–172.
- [113] C. Yi, J. Luo, S. Meloni, A. Boziki, N. Ashari-Astani, C. Grätzel, S. M. Zakeeruddin, U. Röhrlisberger, M. Grätzel, *Energ. Environ. Sci.* **2016**, *9*, 656–662.
- [114] Z. Li, M. Yang, J. Park, S. Wei, J. J. Berry, K. Zhu, *Chem. Mater.* **2016**, *28*, 284–292.
- [115] M. Saliba, T. Matsui, J. Seo, K. Domanski, J. Correa-Baena, M. K. Nazeeruddin, S. M. Zakeeruddin, W. Tress, A. Abate, A. Hagfeldt, M. Grätzel, *Energ. Environ. Sci.* **2016**, *9*, 1989–1997.
- [116] R. M. DeVries, K. I. Kubo, *Phys. Rev. Lett.* **1973**, *30*, 325–328.
- [117] J. Calabrese, N. L. Jones, R. L. Harlow, N. Herron, D. L. Thorn, Y. Wang, *J. Am. Chem. Soc.* **1991**, *113*, 2328–2330.
- [118] I. C. Smith, E. T. Hoke, D. Solis-Ibarra, M. D. McGehee, H. I. Karunadasa, *Angew. Chem. Int. Ed.* **2014**, *53*, 11232–11235; *Angew. Chem.* **2014**, *126*, 11414–11417.
- [119] L. N. Quan, M. Yuan, R. Comin, O. Voznyy, E. M. Beauregard, S. Hoogland, A. Buin, A. R. Kirmani, K. Zhao, A. Amassian, D. H. Kim, E. H. Sargent, *J. Am. Chem. Soc.* **2016**, *138*, 2649–2655.
- [120] D. H. Cao, C. C. Stoumpos, O. K. Farha, J. T. Hupp, M. G. Kanatzidis, *J. Am. Chem. Soc.* **2015**, *137*, 7843–7850.
- [121] D. B. Mitzi, *J. Mater. Chem.* **2004**, *14*, 2355–2365.
- [122] T. M. Koh, V. Shanmugam, J. Schlipf, L. Oesinghaus, P. Müller-Buschbaum, N. Ramakrishnan, V. Swamy, N. Mathews, P. P. Boix, S. G. Mhaisalkar, *Adv. Mater.* **2016**, *28*, 3653–3661.
- [123] K. Yao, X. Wang, F. Li, L. Zhou, *Chem. Commun.* **2015**, *51*, 15430–15433.
- [124] N. D. Marco, H. Zhou, Q. Chen, P. Sun, Z. Liu, L. Meng, E. Yao, Y. Liu, A. Schiffer, Y. Yang, *Nano Lett.* **2016**, *16*, 1009–1016.
- [125] G. Kieslich, S. Sun, A. K. Cheetham, *Chem. Sci.* **2014**, *5*, 4712–4715.
- [126] M. Szafranski, M. Jarek, *CrystEngComm* **2013**, *15*, 4617–4623.
- [127] G. Giorgi, J. Fujisawa, H. Segawa, K. Yamashita, *J. Phys. Chem. C* **2015**, *119*, 4694–4701.
- [128] H. Hsu, C. Chang, C. Chen, B. Jiang, R. Jeng, C. Cheng, *J. Mater. Chem. A* **2015**, *3*, 9271–9277.
- [129] Y. Ogomi, A. Morita, S. Tsukamoto, T. Saitho, Q. Shen, T. Toyoda, K. Yoshino, S. S. Pandey, T. Ma, S. Hayase, *J. Phys. Chem. C* **2014**, *118*, 16651–16659.
- [130] N. Mercier, *CrystEngComm* **2005**, *7*, 429–432.
- [131] D. Bi, P. Gao, R. Scopelliti, E. Oveisi, J. Luo, M. Grätzel, A. Hagfeldt, M. K. Nazeeruddin, *Adv. Mater.* **2016**, *28*, 2910–2915.
- [132] J. Carrillo, A. Guerrero, S. Rahimnejad, O. Almora, I. Zarazua, E. Mas-Marza, J. Bisquert, G. Garcia-Belmonte, *Adv. Energy Mater.* **2016**, *6*, 1502246.
- [133] D. B. Mitzi, C. D. Dimitrakopoulos, J. Rosner, D. R. Medeiros, Z. T. Xu, C. Noyan, *Adv. Mater.* **2002**, *14*, 1772–1776.
- [134] A. Buin, R. Comin, J. Xu, A. H. Ip, E. H. Sargent, *Chem. Mater.* **2015**, *27*, 4405–4412.
- [135] S. Dharani, H. A. Dewi, R. R. Prabhakar, T. Baikie, C. Shi, D. Yonghua, N. Mathews, P. P. Boix, S. G. Mhaisalkar, *Nanoscale* **2014**, *6*, 13854–13860.
- [136] Q. Wang, M. Lyu, M. Zhang, J. Yun, H. Chen, L. Wang, *J. Phys. Chem. Lett.* **2015**, *6*, 4379–4384.
- [137] A. D. Sheikh, A. Bera, M. A. Haque, R. B. Rakhi, S. D. Gobbo, H. N. Alshareef, T. Wu, *Sol. Energy Mater. Sol. Cells* **2015**, *137*, 6–14.
- [138] R. Li, X. Xiang, X. Tong, J. Zou, Q. Li, *Adv. Mater.* **2015**, *27*, 3831–3835.
- [139] X. Xu, Y. Chen, L. Dai, *Nat. Commun.* **2015**, *6*, 8103.
- [140] Y. Chen, T. Chen, L. Dai, *Adv. Mater.* **2015**, *27*, 1053–1059.
- [141] S. A. Kulkarni, T. Baikie, P. P. Boix, N. Yantara, N. Mathews, S. Mhaisalkar, *J. Mater. Chem. A* **2014**, *2*, 9221–9225.
- [142] P. Fedeli, F. Gazza, D. Calestani, P. Ferro, T. Besagni, A. Zappettini, G. Calestani, E. Marchi, P. Ceroni, R. Mosca, *J. Phys. Chem. C* **2015**, *119*, 21304–21313.
- [143] B. Suarez, V. Gonzalez-Pedro, T. S. Ripolles, R. S. Sanchez, L. Otero, I. Mora-Sero, *J. Phys. Chem. Lett.* **2014**, *5*, 1628–1635.
- [144] F. Bella, A. Sacco, G. P. Salvador, S. Bianco, E. Tresso, C. F. Pirri, R. Bongiovanni, *J. Phys. Chem. C* **2013**, *117*, 20421–20430.
- [145] X. Liu, Z. Cao, H. Huang, X. Liu, Y. Tan, H. Chen, Y. Pei, S. Tan, *J. Power Sources* **2014**, *248*, 400–406.
- [146] Y. Chen, B. Li, W. Huang, D. Gao, Z. Liang, *Chem. Commun.* **2015**, *51*, 11997–11999.
- [147] Q. Jiang, D. Rebollar, J. Gong, E. L. Piacentino, C. Zheng, T. Xu, *Angew. Chem. Int. Ed.* **2015**, *54*, 7617–7620; *Angew. Chem.* **2015**, *127*, 7727–7730.
- [148] H. L. Clever, F. J. Johnston, *J. Phys. Chem. Ref. Data* **1980**, *9*, 751.
- [149] G. W. Leonard, M. E. Smith, D. N. Hume, *J. Phys. Chem.* **1956**, *60*, 1493–1495.
- [150] Q. Tai, P. You, H. Sang, Z. Liu, C. Hu, H. L. W. Chan, F. Yan, *Nat. Commun.* **2016**, *7*, 11105.
- [151] A. M. Ganose, C. N. Savory, D. O. Scanlon, *J. Phys. Chem. Lett.* **2015**, *6*, 4594–4598.
- [152] Y. Zhang, S. Chen, P. Xu, H. Xiang, X. Gong, A. Walsh, S. Wei, arXiv preprint **2015**, arXiv:1506.01301.

Received: April 16, 2016





Published online: ■ ■ ■ ■ ■ ■ ■ ■ ■ ■



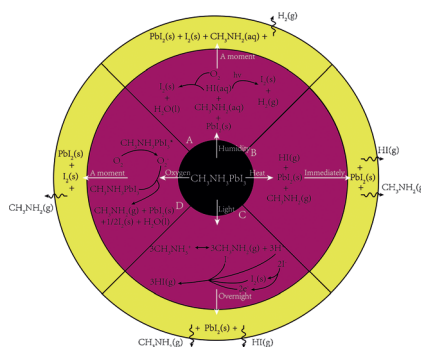
Reviews

Solar Cells

Z. Wang, Z. Shi, T. Li, Y. Chen,*

W. Huang*    

Stability of Perovskite Solar Cells: A
Prospective on the Substitution of the
A Cation and X Anion



Stability rising: The recent advances in improving the chemical stability of perovskite materials in terms of substitution of A-cation and X-anion are reviewed. The aim is to open new perspectives for the rational design of perovskite materials to create perovskite solar cells with unprecedented stability for outdoor applications.